Physics – Uspekhi **64** (12) 1261 – 1285 (2021)

REVIEWS OF TOPICAL PROBLEMS

PACS numbers: 95.30.Cq, 95.55.Vj, 98.70.Vc

50th ANNIVERSARY OF THE INSTITUTE FOR NUCLEAR RESEARCH, RAS

Constraints on models of the origin of high-energy astrophysical neutrinos

S V Troitsky

DOI: https://doi.org/10.3367/UFNe.2021.09.039062

Contents

Abstract. The existence of astrophysical neutrinos with energies of tens of TeV and higher has been firmly established by the IceCube experiment; the first confirmations of this discovery were obtained by the ANTARES and Baikal-GVD installations. At the same time, observational results do not fully agree with those expected before the start of these experiments. The origin of the neutrino has not yet been determined, while simple theoretical models, popular for decades, cannot explain the entire ensemble of observational data. In the present review, a summary of experimental results is given with a particular emphasis on those most relevant for constraining theoretical models; features of various scenarios of the origin of high-energy neutrinos are discussed; and particular classes of their potential astrophysical sources are briefly listed. It is shown that observational data may be explained if the astrophysical neutrino flux includes both a contribution of extragalactic sources, dominant at high energies, and a Galactic component, essential only at neutrino energies $\lesssim$ 100 TeV. Other possible scenarios are also discussed.

Keywords: neutrino, multimessenger astrophysics, high-energy astronomy

S V Troitsky
Institute for Nuclear Research, Russian Academy of Sciences,
prosp. 60-letiya Oktyabrya 7a, 117312 Moscow, Russian Federation
E-mail: st@ms2.inr.ac.ru

Received 2 July 2021, revised 7 September 2021
Uspekhi Fizicheskikh Nauk **191** (12) 1333 – 1360 (2021)
Translated by S V Troitsky

1. Introduction

1.1 Astrophysical high-energy neutrinos: formulation of the problem

Modern astrophysics has confidently moved beyond the so-called photon channel: the study of sources based on the electromagnetic radiation of various bands coming from them. The first extraterrestrial sources of neutrinos, the Sun and supernova 1987A, and then also gravitational waves, have been detected. Extraterrestrial charged particles, cosmic rays, are being studied intensively. Along with the development of electromagnetic astronomy, including the highest energies at which telescopes detect individual photons, this gave rise to so-called multimessenger astrophysics, which uses different carriers — photons, neutrinos, charged particles, and gravitational waves — to obtain information about the structure of astrophysical objects and about physical processes going on in them. Here, we will focus on one of the channels of multimessenger astronomy, the detection of high-energy neutrinos, and related observations in other channels.

Due to the unique place of the neutrino among elementary particles (a stable particle experiencing weak interactions only), the main goal of neutrino astronomy in the 20th century was the study of sources opaque to electromagnetic radiation. Thus, the discovery of solar neutrinos experimentally proved that the energy of the Sun comes from thermonuclear reactions in its central region not accessible to other observations, and the registration of neutrinos from supernova 1987A allowed us to verify our understanding of physical processes taking place in the interior of a massive star upon the gravitational collapse of its core. In both cases, neutrinos are born in nuclear processes and have energies

corresponding to characteristic nuclear scales (from fractions to tens of MeV). Occurring in substantially opaque regions, these processes 'heat' the source and are eventually related to thermal electromagnetic radiation — for example, solar radiation.

At the same time, a large portion of the photon radiation in the Universe is associated with nonthermal processes and is determined by the interaction of relativistic particles with ambient fields, matter, and radiation. As a rule, such nonthermal emission at relatively low energies, from radio to ultraviolet, and sometimes up to the X-ray band, is well explained by the synchrotron radiation of relativistic electrons. At higher energies, the situation becomes less clear — along with the synchrotron radiation of electrons, inverse-Compton radiation may be significant, as might be the proton synchrotron or photon production in elementary particle interactions. Since the only way to produce astrophysical neutrinos with energies $\gtrsim 10$ GeV that does not involve nonstandard physics or astrophysics is the interaction of high-energy protons (see Section 3.1), the role of neutrinos in astronomy changes with the transition to high energies — instead of being carriers of information about processes in opaque media, they become markers of interactions of relativistic hadrons whose acceleration to high energies requires the medium to be not too dense.

This transition from neutrinos born in nuclear processes to neutrinos associated with high-energy elementary particle interactions is crucial in distinguishing high-energy neutrino astrophysics as a separate field, to which this review is devoted. Note that one article, even a large one, cannot fully cover all aspects of this actively developing area. This review, therefore, does not purport to be complete. We will concentrate on astrophysical models of the origin of neutrinos with energies in the $10^{11}-10^{16}$-eV range and will therefore focus only on the most relevant experimental results for their study. Beyond the scope of this work are, in particular, ultrahigh energy neutrinos, interesting details of the experimental work on neutrino detection, and various results in a certain way related to the study of elementary particle properties. Even within this framework, a review of the literature will be necessarily incomplete, for which the author apologizes in advance. Books and reviews [1–6] and others that touch on a variety of aspects of high-energy neutrino astronomy can be recommended to the reader.

1.2 High-energy neutrino detection

1.2.1 Neutrino interactions in water. The experimental data to be discussed in this article were obtained using neutrino telescopes that record Cherenkov emission of charged particles, the products of neutrino interactions in large volumes of water (in the solid or liquid state). Interactions of neutrinos with q quarks of nucleons of target atomic nuclei can proceed with a W-boson exchange (charged current, CC),

$$\mathrm{CC}:\ \nu_l + \mathrm{q} \to l + X, \tag{1}$$

where ν_l and l are neutrinos and charged leptons of the same flavor, $l = \mathrm{e}, \mu, \tau$, and X denotes other hadronic products of the reaction. The other interaction channel is the Z-boson exchange (neutral current, NC),

$$\mathrm{NC}:\ \nu_l + \mathrm{q} \to \nu_l + X. \tag{2}$$

Similar reactions are possible for antineutrinos.

The probability of interaction between neutrinos and target electrons is low except in the case of so-called Glashow resonance [7, 8], the direct production of a W-boson,

$$\bar{\nu}_\mathrm{e} + \mathrm{e} \to \mathrm{W} \to \ldots, \tag{3}$$

where '...' denotes a well-studied set of W-boson decay products which can include both hadrons and leptons. This process goes only for antineutrinos, for there are no positrons in the target. Resonance occurs at energy $E_{\bar{\nu}_\mathrm{e}} = m_\mathrm{W}^2/(2m_\mathrm{e})$, where m_W and m_e are the masses of the W-boson and electron, respectively.

The result of the interactions observed in the detector depends not only on the type (1)–(3), but also on the flavor of the initial neutrino. The CC reaction involving ν_μ ($\bar{\nu}_\mu$) results in the production of a relativistic muon, whose decay length is, at the energies of interest, usually larger than the size of the detector. The Cherenkov radiation of this single muon is recorded as a narrow track crossing the detector. Note that the widespread notion that such track events are associated only with ν_μ is not entirely correct: they also include muons from the decay of τ-leptons born in CC interactions of ν_τ or from $\mathrm{W} \to \mu^- \bar{\nu}_\mu$ in the case of Glashow resonance, as well as high-energy τ-leptons that do not have time to decay in the detector (a total of $\sim 10\%$ of all tracks [9]).

CC events involving ν_e or $\bar{\nu}_\mathrm{e}$ lead to the formation in the detector of two multiparticle processes that overlap and form a common cascade. One of the showers starts with the braking radiation of the electron, whose radiative length in water is only about 36 cm, and the other is associated with the hadronic products of X. Note that the longitudinal development of the cascade occurs over a length three orders of magnitude shorter than the length of the muon track (see, e.g., estimates in Ref. [3]).

The CC reaction caused by ν_τ or $\bar{\nu}_\tau$ looks different in the detector, depending on the neutrino energy. The decay length of a τ-lepton with energy E_τ is $\sim 50\ \mathrm{m} \times (E_\tau/\mathrm{PeV})$, so at PeV energies this event is observed as a double cascade [10] — at the interaction point, a shower of X hadrons is recorded, and at the decay point, one from τ decay products, also predominantly hadronic. It is possible to separate the showers both spatially and by the time interval between two flashes [11]. At energies of $\lesssim$ PeV, these interactions look like normal cascades.

Finally, at NC interactions of neutrinos and antineutrinos of all types, only the hadronic cascade is recorded, as the neutrino remaining in the final state leaves the detector undetected.

1.2.2 Specifics of observing track and cascade events. Events interpreted as Glashow resonance or a double cascade are associated with the highest neutrino energies and thus are very rare [12, 13], so the bulk of astrophysically interesting information is associated with tracks and cascades. In practice, the registration of Cherenkov radiation is made by a three-dimensional array of optical modules with photodetectors viewing a large volume of the target. In order to reduce the background from muons of extensive atmospheric showers (see later in this section), the facility is immersed in water (ice) to a depth of at least one kilometer. Photodetectors record the amount of Cherenkov light and, with high accuracy, the moment of a flash. The latter is important, because the temporal evolution of the signal makes it possible to determine the direction and speed of a muon or of cascade

Table 1. Comparison of water and ice detectors. Longer length corresponds to better optical performance.

	Lake Baikal water	Salt water	Ice
Absorption length, m	~ 20	~ 50	~ 100
Scattering length, m	~ 200	~ 200	20–40
Problems	Shallower available depth, bioluminescence, chemiluminescence	Radioactivity of dissolved salts, bioluminescence, chemiluminescence	Dust inclusions, clathrates

development. Illustrations with images of simulated and real recorded events can be found in the reviews cited above, popular science literature (see, e.g., [14]), and the media.

The cascade evolves almost isotropically in the center-of-mass system of the original particles, so in the laboratory frame it looks like an extended 'cloud.' The neutrino arrival direction is determined considerably worse in this case than for a long linear muon track; see examples below. In contrast, in terms of the energy determination, cascades are indispensable: if a cascade begins in the working volume of the detector (so-called starting events), then almost all of the energy of the initial neutrino goes to Cherenkov light and is collected by photodetectors.

For track events, the potential of determining the energy of the initial neutrino is noticeably more modest. The muon track usually extends beyond the boundaries of the facility, so the total recorded energy release in the detector, $E_{\rm dep}$, gives only a lower bound on the muon energy E_μ at the entrance to the detector, which is estimated using the time evolution of the signal. Since it is not known how much energy the muon has lost before entering the detector, nor how much of the energy of the original neutrino was transferred to the muon, this measurement allows estimating the energy of the muon at birth $\hat{E}_\mu$ and the energy of the original neutrino E_ν only in a statistical way. While E_ν is constrained from below quite well, the broad non-Gaussian distribution of possible E_ν corresponding to a given muon detection extends towards values of E_ν orders of magnitude higher (Fig. 1). Additionally, note that this statistical distribution, as well as the most likely estimate of E_ν, depends on the assumption about the spectrum of astrophysical neutrinos.

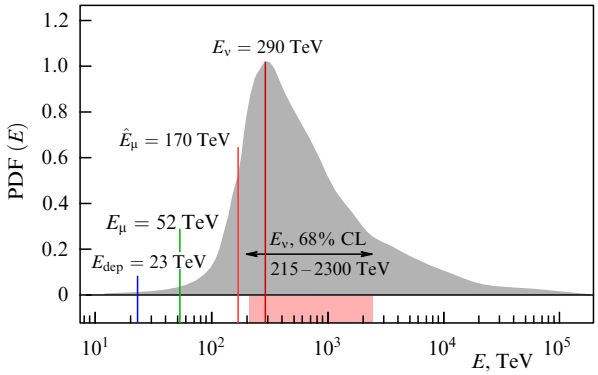

Figure 1. Illustration of the energy-estimate uncertainty for a track event using the example of one of the best known neutrinos registered by IceCube (IC170922A, coincident with the outburst of the blazar TXS 0506+056; see Section 2.3.4). Horizontal axis: energy deposited in the detector $E_{\rm dep} = 23.7 \pm 2.8$ TeV, reconstructed energy of the muon entering the detector $E_\mu = 52^{+11}_{-9}$ TeV, energy estimate of the muon at birth $\hat{E}_\mu \simeq 170$ TeV, most likely neutrino energy $E_\nu \simeq 290$ TeV. The shaded graph shows the probability density function (PDF) of the values of E_ν; also shown is the uncertainty region of the E_ν values — from 215 to 2300 TeV (68% CL). A power-law spectrum of astrophysical neutrinos with exponent 2.13 is assumed. Plotted on the basis of data from Ref. [15].

1.2.3 Arrival directions. Water and ice. In particle-physics terms, the interactions of neutrinos in liquid water and in ice are of course identical, but for the detection of Cherenkov radiation and for event reconstruction, the properties of these media are quite different.

Table 1 gives the characteristic values of the absorption and scattering lengths of light at wavelengths of the maximal Cherenkov radiation for typical experimental conditions in different media (for details, see Refs [5, 16]). Under real conditions, these values strongly depend on the specific location, primarily on the depth, varying even within the same installation. Nevertheless, the averaged estimates show that the instruments using liquid water and ice complement each other. In terms of identifying events and measuring their energies, ice is more convenient — it has less illumination from natural sources (bio- and chemiluminescence and radioactivity), and the weak absorption allows one to collect more light from each event, lowering the registration threshold and increasing the accuracy of the energy determination. In contrast, for the astrophysical task of identifying neutrino sources, the accuracy of the arrival direction, including both the statistical scatter and systematic errors, is of more importance. The statistical errors are largely determined by the scattering length, so that they are about 5 times smaller in water experiments than in ice experiments; this is true for both cascades and tracks. In the case of cascade events, this improvement (from $15^\circ - 20^\circ$ to $3^\circ - 4^\circ$) is crucial.

Another important component of the accuracy of the reconstruction of neutrino arrival directions is systematic uncertainties. They come primarily from the accuracy of positioning the detector as a whole and from imperfections in the reconstruction of events, including insufficient knowledge of the properties of the medium. Since inhomogeneities, bubbles, and inclusions in water mix, float, or settle down, the working volume of a water detector is much more homogeneous and much more uniform and controllable than that of an ice detector. If the accuracy of absolute positioning can be estimated from observation of the shadow of the Moon, the second component of the systematic uncertainties is much harder to estimate. Some estimates of its magnitude may be obtained by comparing the arrival directions of the same events reconstructed with different algorithms and with different ice models (Figs 2 and 3), where also some typical statistical errors in determining the neutrino arrival directions are shown.

1.2.4 Passage of neutrinos through Earth. Neutrino interaction cross sections increase with energy, and at the high energies of interest, Earth is no longer completely transparent to neutrinos. For different arrival directions, paths through Earth are different, but the dependence of the interaction probability is not just geometric, because Earth has a very dense core with a sharp boundary. This issue is discussed in

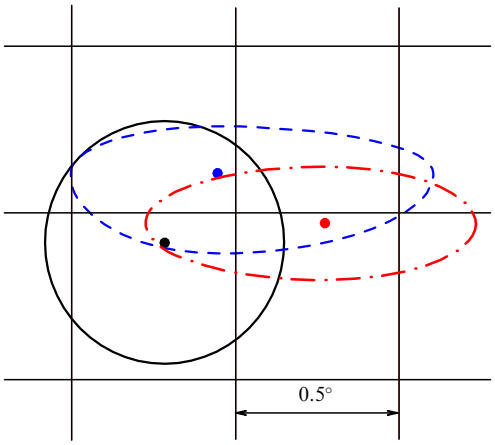

Figure 2. Illustration of statistical and systematic uncertainties of arrival directions of track events. Arrival directions and their 90% CL statistical error regions are shown for the same event with an energy of ~ 4450 TeV, according to Ref. [17] (dashed-dotted line), the catalog of alert events [18] (dashed line), and the IceCube 10-year public catalog [19, 20] (solid line). Difference between reconstructions gives an estimate of the systematic uncertainty.

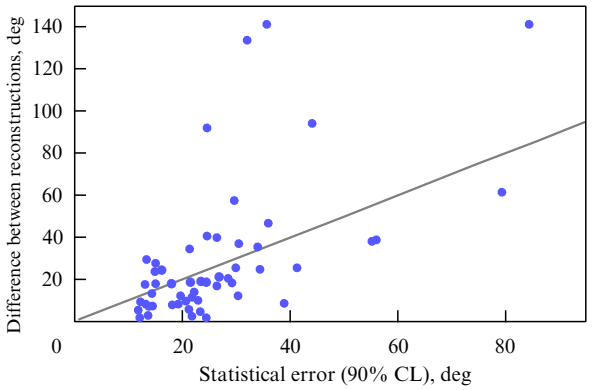

Figure 3. Illustration of statistical and systematic uncertainties of arrival directions of cascade events. Horizontal axis gives the value of the statistical error (90% CL) of the arrival direction of HESE cascades of Refs [21–23]; vertical axis gives the difference between the arrival directions of these events in the original [21–23] and new [24] reconstructions.

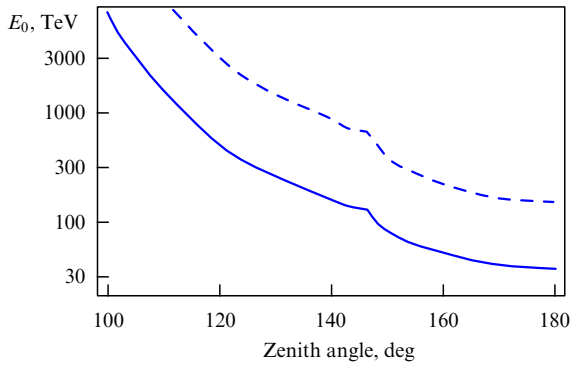

Figure 4. Critical energy E_0 for which the optical depth for an electron neutrino with respect to its interaction with Earth's matter is 1 (solid line) or 2.3 (dashed line, 90% of neutrinos interact) as a function of the zenith angle. At energies $\gtrsim E_0$, Earth gradually becomes opaque to neutrinos coming from this direction.

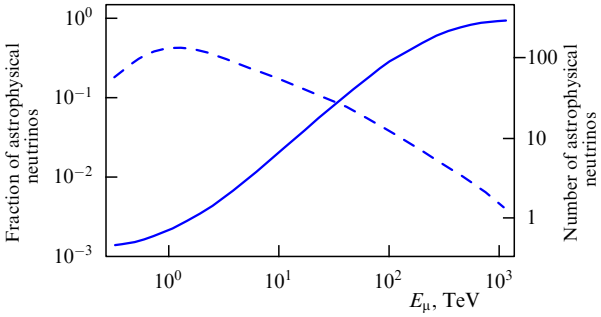

Figure 5. Expected fraction of astrophysical neutrinos in the total number of muon tracks as a function of energy E_μ (left scale, solid line) and the expected total number of astrophysical neutrinos at a given energy (per 0.1 dex bin in E_μ, right scale, dashed line) in a set of $\sim 650{,}000$ IceCube events. Plotted with the data from Ref. [25] (model for 10 years of observations).

more detail in Refs [1, 3]; here, we present only Fig. 4, plotted on the basis of the data from these studies. It shows the characteristic neutrino energy, from which interaction with Earth is significant, as a function of the zenith angle. Note that some of the interactions are elastic, after which the neutrino continues its motion with lower energy, so that the total flux suppression also depends on the spectrum of the incoming particles, not only on the zenith angle.

1.2.5. Atmospheric and astrophysical neutrinos. The main backgrounds for detecting astrophysical neutrinos are muons and neutrinos from interactions of cosmic rays with Earth's atmosphere. Other than at the highest energies, this background dominates the signal. For instance, Fig. 5 gives an estimate of the fraction of astrophysical events in the set of IceCube muon tracks as a function of muon energy E_μ. Despite such a modest signal-to-background ratio, there are ways to isolate the astrophysical component in the analysis.

For energies of the order of GeV, the process of atmospheric neutrino production in interactions of cosmic rays with hadrons present in the atmosphere is quite similar to the mechanism of the origin of astrophysical neutrinos in pp interactions (see Section 3.1 below): $\pi^\pm$ mesons are born and then decay, and then the $\mu^\pm$, produced at this first stage, decay as well. The resulting neutrino spectrum reflects the spectrum of cosmic rays, $E^{-2.7}$, and the flavor ratio $\nu_e:\nu_\mu:\nu_\tau$ is 1:2:0. The situation changes for muon energies $\hat{E}_\mu \gtrsim 10$ GeV, when the muons begin to reach Earth's surface without decay. As a result, the flavor composition changes so that the ratio $\nu_e:\nu_\mu$ becomes $\sim 1:30$ (electron neutrinos are born in some K-meson decays; ν_τ still has no mechanism to be produced). In addition, at π-meson energies $E_\pi \gtrsim 100$ GeV, π mesons have no time to decay either — they interact faster with atmospheric hadrons; atmospheric showers begin to develop. Since the decay probability falls with energy as $1/E_\pi$ (Lorentz kinematics), and the interaction probability weakly depends on the energy, in the energy region of interest, the spectrum of atmospheric neutrinos from π- and K-meson decays follows $\sim E^{-3.7}$ (see Section 2.2 below for a discussion of the contribution of charmed hadrons).

The distribution of atmospheric neutrinos in zenith angles peaks strongly for horizontal directions, since in this case the muon's path in the atmosphere is longer, and hence it is more

Table 2. Major experiments in high-energy neutrino astrophysics. Specified are the years physical results were obtained, including incomplete configuration.

Name	Location	Volume, km^3	Years	Note
HT-36 HT-200 HT-200+	Lake Baikal	10^{-4} (*)	1993 – 2015	First detection of muon tracks from atmospheric neutrinos
AMANDA	South Pole	0.015	1996 – 2008	Atmospheric neutrino spectrum up to $\sim$ 100 TeV and constraints on astrophysical models
ANTARES	Mediterranean Sea	0.025 (*)	2006 – ...	
IceCube	South Pole	1.0	2006 – ...	Observation of astrophysical neutrinos. Largest number of statistics (2021)
Baikal-GVD	Lake Baikal	0.4 (2021) (*) $\geqslant$ 1 (plan)	2016 – ...	Data taking in process of deployment
KM3NeT	Mediterranean Sea	$\sim$ 1 (*) (plan)	2019 – ...	
IceCube-Gen2	South Pole	$\sim$ 10 (plan)	Project	
P-ONE	Pacific Ocean, Canada	$\sim$ 3 (*) (plan)	Project	

(*) Volume filled with detecting equipment; water detectors can be used to record high-energy cascades in the volume well in excess of these values.

likely to decay. In real analyses at high energies, this dependence is further strengthened by applying the muon veto for events coming from above (events with simultaneous signals from other muons from the same shower are rejected), while for $E_\nu \gtrsim 50$ TeV, Earth's opacity to neutrinos starts to be noticeable for events coming from below. It is the combination of the very soft spectrum $E^{-3.7}$ and the described dependence on the zenith angle which gives the basis for the extraction of the astrophysical signal against the atmospheric background on a statistical basis; see Section 2.1 below.

1.3 Past, present, and future experiments

The idea of underwater detection of high-energy neutrinos was first proposed by M A Markov and I M Zheleznykh [26] (see also Ref. [27]). It is not the purpose of this review to discuss in detail the history of neutrino astronomy, nor to give a detailed technical description of the instruments at work (see Refs [2, 4, 5] and references therein). Brief information about past, present, and emerging detectors, which may be useful in reading the rest of the review, can be found in Table 2.

2. Principal experimental results

2.1 Extraterrestrial origin of neutrinos

As has already been noted, we are discussing neutrinos with energies substantially above nuclear scales. There are no terrestrial sources of such neutrinos (except for narrow beams of neutrinos of accelerator origin, which, however, do not enter into experimental facilities of the cubic-kilometer scale). The astrophysical signal in the detectors should be separated from atmospheric neutrinos produced by the interaction of cosmic rays with Earth's atmosphere, and from background events caused by muons from the same interactions. When studying a single neutrino event, it is not possible to say definitively whether it was of atmospheric or astrophysical origin, but in examining the ensemble of data it is possible to distinguish the astrophysical component of the flux from the atmospheric one. For this purpose, one uses the distribution of events in energies (at high energies, hard

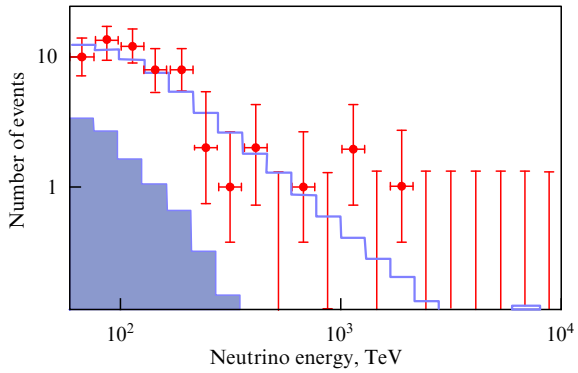

Figure 6. Distribution of IceCube cascade events, starting in the detector, in the energy deposited in the detector ($E > 60$ TeV). Red dots with error bars — data, dark shading — standard atmospheric background, solid line — fit of the sum of the background and the astrophysical component. Plotted with data from Ref. [24].

astrophysical spectra become more pronounced than soft atmospheric ones: Fig. 6) and the zenith angle (Fig. 7). While astrophysical neutrinos come fairly isotropically (only at the highest energies does Earth become opaque to them), the distribution of atmospheric neutrinos by zenith angles peaks for horizontal directions. The atmospheric muons themselves can be filtered out by a simultaneous triggering system mounted on the surface, or — for directions from below — simply by Earth.

Detection of neutrinos of astrophysical origin was first announced by the IceCube Collaboration in 2013 based on the observation of two events with cascades started in the detector with reconstructed energies above 1 PeV, for which the atmospheric background is simply negligible. Presently, various analyses based on IceCube datasets with different selection criteria are being carried out, and in all of them the presence of an astrophysical component of the neutrino flux has been established in a statistically significant way, based on a combination of multiple factors. For the most energetic individual events, the probability of their astrophysical origin has been determined (we note that for particular samples used

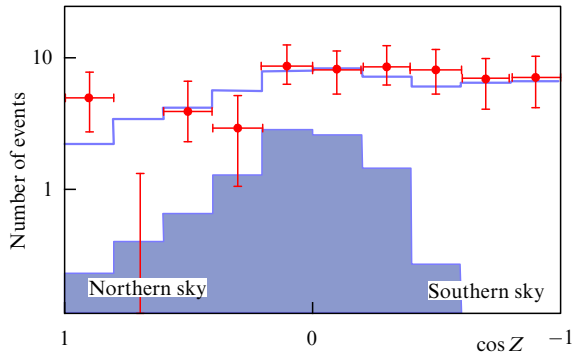

Figure 7. Distribution of IceCube cascade events ($E > 60$ TeV), starting in the detector, at the zenith angle Z. Red dots with error bars — data, dark shading — standard atmospheric background, solid line — fit of the sum of the background and the astrophysical component. Plotted with data from Ref. [24].

in the IceCube analyses, even for those selected according to the most stringent criteria, this probability does not exceed $\sim 60\%$ on average).

An independent confirmation of the presence of astrophysical neutrinos by other experiments should be considered an important step in the development of neutrino astrophysics. Such a result, albeit with low statistical confidence, was presented in 2019 by the ANTARES collaboration [28]. The number of events with energies above 100 TeV recorded at the Baikal-GVD facility during data taking in the incomplete configuration is also consistent with the presence of the astrophysical neutrino flux with the parameters measured by IceCube [29]. An eagerly awaited, more accurate, quantitative verification of the IceCube results will be possible after a few years of Baikal-GVD's work.

2.2 Spectrum and flavor composition

Detailed measurements of the spectrum of astrophysical neutrinos, similar to those carried out for cosmic rays, are still difficult because of statistical and systematic uncertainties. The energies of individual track events are estimated with low accuracy, which does not allow any meaningful binning of the spectrum, while the number of reliably studied cascade events is small. In addition, the estimation of the astrophysical flux (F) is always based on subtracting the atmospheric background, which is also modeled with uncertainties. As a consequence, most of the spectrum estimates obtained so far use a simple power-law fit,

$$\frac{\mathrm{d}F_{\nu+\bar{\nu}}}{\mathrm{d}E_\nu} = \Phi_0 \left(\frac{E_\nu}{100\ \mathrm{TeV}}\right)^{-\gamma} \times 10^{-18}\ \mathrm{GeV}^{-1}\ \mathrm{cm}^{-2}\ \mathrm{s}^{-1}\ \mathrm{sr}^{-1}, \quad (4)$$

where the fit parameters are the normalization Φ_0 and the exponent γ. The standard parameterization (4) refers to the diffuse isotropic flux of neutrinos and antineutrinos of the same flavor, defined assuming equal fluxes of all six types of neutrinos and antineutrinos (thus, the total flux is obtained by multiplying that given by Eqn (4) by three). Different analyses are more or less sensitive to different energy intervals and different flavors. Parameters of the best-fit spectrum (4), determined in the various IceCube and ANTARES analyses, are given in Table 3. The ranges of energies, which make the main (usually 90%) contribution to the fit spectrum, are also indicated. A more detailed discussion of the features of the datasets used and of details of the experimental work is beyond the scope of this paper; a rather detailed description of different IceCube analyses is given in a recent paper [24].

Although the parameters of the spectra obtained in the different analyses are close to each other in order of magnitude, their scatter is strikingly greater than the 68% confidence intervals indicated in Table 3. Errors in the parameters Φ_0 and γ are not completely independent, so the contours of the confidence regions in the plane of these two parameters are often compared (see, e.g., [24]). Such a comparison does not always seem to be optimal due to the fact that the energy intervals used in the analyses are different, and the true spectrum is probably different from the exact power law. This latter possibility is supported by a visual comparison of the power-law fitted spectra plotted for the energy ranges of the respective analyses (Fig. 8). It can be seen that, on average, the spectra become harder at higher energies, and at a fixed energy agreement between those analyses which have sufficient statistics in this region are not bad. The neutrino fluxes fall rapidly with energy in any case, so the best statistics saturating the fit are obtained closer to the lower boundary of the energy range in use. It is natural to attribute the 'measurement' of the γ power-law index to the average energy of events contributing to the fit, which is easy to estimate by knowing the γ value itself and the energy range. The results of this estimate are shown in Fig. 9. The tendency for the spectrum to become harder with increasing energy is particularly clear in this representation — only one point [24] drops out, which, however, is based on only 60 events, albeit of high quality. Possible reasons for this behavior of the spectrum deserve a more detailed discussion, to which we now turn.

Atmospheric background? As discussed above, isolating the contribution of astrophysical neutrinos in the background of atmospheric neutrinos at high energies is quite easy: astrophysical neutrinos have a harder spectrum and a different distribution of zenith angles (see Figs 6 and 7). However, this applies to so-called standard atmospheric neutrinos from

Table 3. Parameters of power-law fit (4) spectra of astrophysical neutrinos from various IceCube and preliminary ANTARES analyses.

Analysis	Energy	Φ_0	γ
HESE 2020 [24]	69.4 TeV – 1.9 PeV	$2.12^{+0.49}_{-0.54}$	$2.87^{+0.20}_{-0.19}$
Cascades $\nu_e + \nu_\tau$ 2020 [30]	16 TeV – 2.6 PeV	$1.66^{+0.25}_{-0.27}$	2.53 ± 0.07
MESE 2014 [31]	25 TeV – 1.4 PeV	$2.06^{+0.4}_{-0.3}$	2.46 ± 0.12
Inelasticity 2018 [32]	3.5 TeV – 2.6 PeV	$2.04^{+0.23}_{-0.21}$	2.62 ± 0.07
ν_μ 2016 [17]	194 TeV – 7.8 PeV	$0.90^{+0.30}_{-0.27}$	2.13 ± 0.13
ν_μ 2019 [25]	40 TeV – 3.5 PeV	$1.44^{+0.25}_{-0.24}$	$2.28^{+0.08}_{-0.09}$
ANTARES 2019 [28]		1.5 ± 1.0	2.3 ± 0.4

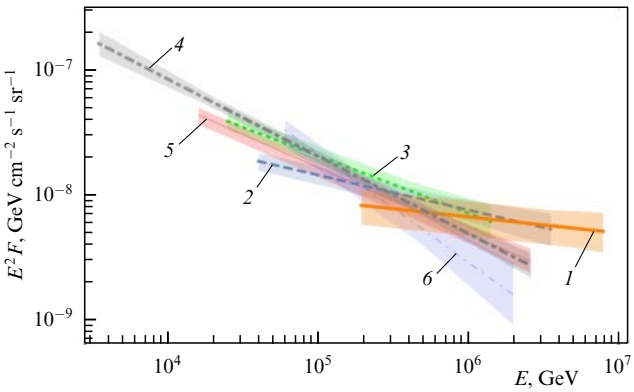

Figure 8. (Color online.) Astrophysical neutrino spectra (4) from various IceCube analyses (for details and references, see Table 3). Thick orange solid line (*1*) — ν_μ 2016; blue dashed line (*2*) — ν_μ 2019; green dotted line (*3*) — MESE 2014; thick gray dashed-dotted line (*4*) — inelasticity 2018; thin red solid line (*5*) — $\nu_e + \nu_\tau$ cascades 2020; thin blue dashed-dotted line (*6*) — HESE 2020. Shading with the corresponding color shows the statistical uncertainties of the corresponding power-law fit.

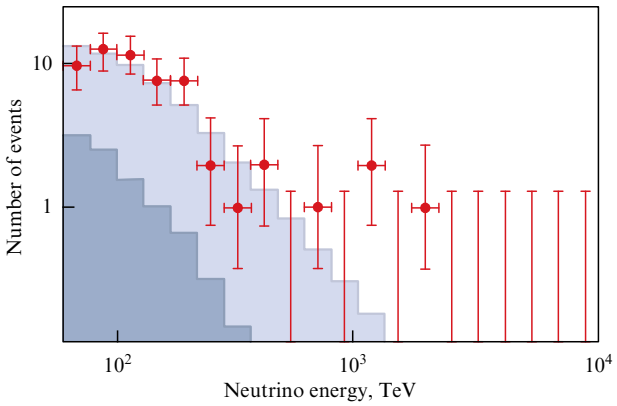

Figure 10. Distribution of IceCube cascade events, starting in the detector, in the energy deposited in the detector ($E > 60$ TeV). Red dots with error bars — data, dark shading — standard atmospheric background, light shading — best fit of the sum of the standard background and the background of prompt atmospheric neutrinos. Plotted with data from Ref. [24].

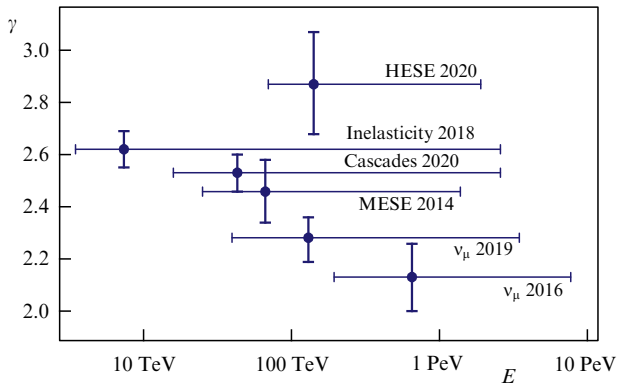

Figure 9. Index of the power-law fit (4) of the astrophysical neutrino spectrum for various IceCube analyses (for the names of the analyses and references, see Table 3). Bold vertical lines show statistical uncertainties of the reconstructed exponents, and thin horizontal lines show the neutrino energy intervals yielding 90% of the events for this analysis. Horizontal positions of the dots correspond to the average energy of the events in the data set, estimated from the power-law fit.

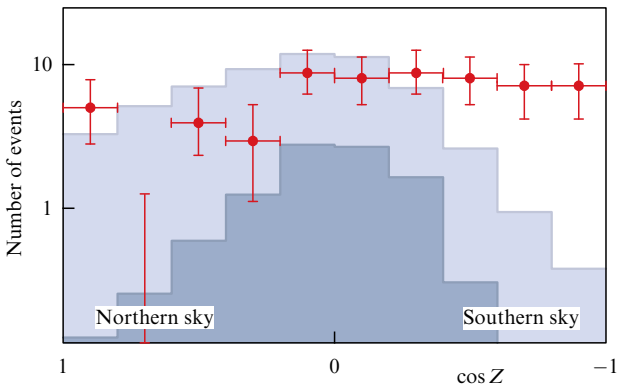

Figure 11. Distribution of IceCube cascade events ($E > 60$ TeV), starting in the detector, in zenith angle Z. Red dots with error bars — data, dark shading — standard atmospheric background, light shading — best fit of the sum of the standard background and the background of prompt atmospheric neutrinos. Plotted with data from Ref. [24].

decays of π- and K-mesons. At the same time, the products of the interaction of cosmic rays with the atmosphere include charmed mesons, $D_s^{\pm}$, and baryons, Λ_c, whose lifetime is about four orders of magnitude shorter. Their decays produce a so-called prompt atmospheric neutrino flux, which has characteristics much closer to those of the astrophysical flux. In particular, due to the short lifetime, the parent hadrons have no time to interact in the atmosphere even at high energies. As a consequence, prompt neutrinos repeat the spectrum of the initial cosmic rays, $E^{-2.7}$, and are distributed isotropically, up to the effect of passing through Earth and event selection effects. Compared to ordinary atmospheric neutrinos, the prompt flux is substantially enriched in electron flavor. All of this allows hypothesizing [33–35] that only the hard component, found in ν_μ, has an astrophysical origin, while the one derived from the analysis of cascade events, rich in ν_e and having a spectrum closer to $E^{-2.7}$, is explained by prompt atmospheric neutrinos. However, for cascades arriving from above the horizon, one can perform an additional analysis. Atmospheric neutrinos are not born alone: in the same atmospheric shower, muons are also produced, which can also be detected. The requirement of a lack of simultaneous detection of such muons suppresses the contribution of atmospheric neutrinos coming from above, including prompt ones, and the distribution of the events selected in this way becomes anisotropic. Figures 10 and 11 show the best fit of the observed energy and zenith-angle distributions for an HESE sample, assuming a zero astrophysical component — an arbitrary normalization of the prompt neutrino flux is allowed instead. Comparing Figs 6 and 7 indicates that the spectrum is described by prompt neutrinos equally well as by astrophysical neutrinos, but the zenith-angle distribution excludes this explanation at $> 5\sigma$ confidence level. It is worth noting that, for a satisfactory explanation of the spectrum, Fig. 10, the prompt flux normalization was increased by a factor of 21.56 over the predictions of modern theoretical models.

It is pertinent to add that an important criterion for the presence of astrophysical neutrinos is the presence of ν_τ among observed events [1, 33, 36], since, among atmospheric neutrinos, both conventional and prompt, the fraction of ν_τ is very small. Observations of the first candidates for ν_τ events [13] support the astrophysical explanation, but the statistics here are still are very few.

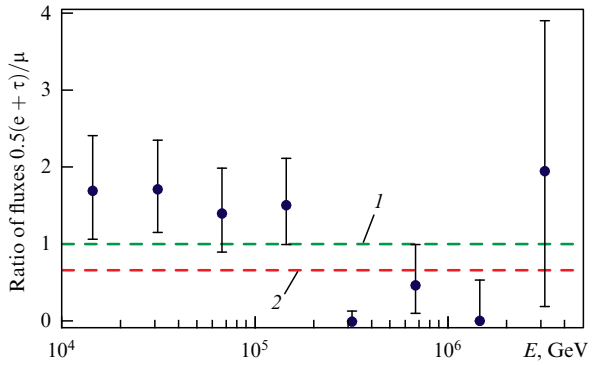

Figure 12. Ratio of neutrino fluxes of different flavors as a function of energy. Average ν_e and ν_τ fluxes are taken from experimental points of the cascade analysis [30, 38], ν_μ, from a power-law fit [25]. Green dashed line (*1*) is unity, predicted in normal π-meson decays, red dashed line (*2*) is 2/3, predicted in the muon damp mode (see Section 3.1).

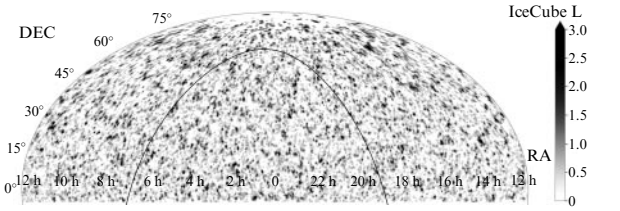

Figure 13. Weighted distribution of IceCube track event arrival directions from below the horizon over 7 years of operation (based on [46, 47]). Likelihood function describing the probability of detecting a source of astrophysical neutrinos in a given direction, taking into account the number of events, the accuracy of determining their arrival directions, and values of the reconstructed energies, is presented. Equatorial coordinates; Galactic plane is shown by a solid black line. RA — right ascension, DEC — declination. The author is grateful to A Plavin for his help in preparing this plot.

Flavor composition? The spectra (4) with parameters from Table 3 were obtained under the assumption of equality of the fluxes of neutrinos of the three flavors. Since in the analyses based on muon tracks the atmospheric background is higher due to the presence of both atmospheric neutrinos and atmospheric muons, the spectra obtained from tracks are dominated by higher energies. Such a systematization can lead to a dependence of the reconstructed energy on the flux, if in fact this assumption is violated (see, e.g., [37]). In Fig. 12, the ratio of the ν_e and ν_τ flux to that of ν_μ, calculated in energy bins [30, 38] from a power-law fit [25] in the energy range common to the two analyses, is given (deviations of the real spectrum from the power law, discussed below, would lead to a change in this picture). It can be seen that at energies $\gtrsim 200$ TeV the results are in poor agreement with the standard assumption of equality between flavors; the agreement does improve if one assumes a transition to a different flavor ratio in this energy range. We will see in Section 3.1 that this may indeed happen for sources with very strong magnetic fields — so strong that it is not easy, though in principle possible, to reconcile the model with other observational data.

At present, the flavor composition of high-energy neutrinos is not very precisely defined, and available results and perspectives are discussed in Refs [39, 40].

North–South anisotropy? Another assumption used in the estimation of the spectra is the isotropy of the diffuse flux. However, none of the approaches to finding astrophysical neutrinos guarantees a uniform sensitivity to the flux coming from different directions. This anisotropy in addition varies with energy, as well as from one analysis to another. Among early attempts to explain the difference in the spectra recovered from cascade and track IceCube events, there were also assumptions about the global anisotropy of neutrino arrival directions (see, e.g., Ref. [41]). Indeed, the track analysis is more sensitive to neutrinos arriving 'from below,' and at the highest energies, close to the horizon; the cascade analysis covers the entire sky and is sensitive to directions 'from above.' The presence of a significant anisotropy of the astrophysical flux, e.g., associated with the dominance of a nearby source in the Southern hemisphere, could explain the observed discrepancy in the spectra. To date, no such anisotropy has been detected. The Northern detectors Baikal-GVD and KM3NeT could definitively rule out or confirm such an explanation, since for them the notions of 'below' and 'above' refer to other parts of the sky.

Two components of the spectrum? In light of what has been said, it would be natural to simply believe that the spectrum over the entire interval of energies investigated differs from the power law (see Fig. 8) and the flux at energies of tens of TeV is higher than expected from the extrapolation of the power law valid above ~ 200 TeV downward in energies. In Section 3, we will see that it is extremely difficult to describe theoretically all the observational data if one assumes the origin of *all* neutrinos with TeV to PeV energies in sources of the same type. The natural next step is to assume two components of the spectrum, one of which (probably extragalactic) has a hard spectrum and extends far into the PeV range, and the other (possibly related to our Galaxy) dominates below $\sim 100-200$ TeV [37, 42–44]. Below, we discuss in more detail the observational motivation for such a hypothesis and possible scenarios for the origin of the two components of the diffuse neutrino flux.

2.3 Arrival directions

To a large extent, methods for studying arrival directions were inherited by high-energy neutrino astronomy from research on cosmic rays of ultra-high, $\gtrsim 10^{18}$ eV, energies (see, e.g., [45]), whose sources are also unknown. These methods include searches for and constraints on large-scale (of the scale of the entire sky) anisotropy, in particular of that related to the Galaxy's disk or halo, and for deviations from the random distribution of arrival directions at angular distances comparable to the telescope's resolution, namely, the search for autocorrelations indicating the existence of point sources, and correlations with specific populations of theoretically justified sources. Unlike for cosmic rays, whose trajectories are deflected by magnetic fields that are often unknown, for neutrinos it is less important to search for medium-scale 'spots' on the celestial sphere, but a new possibility of spatiotemporal correlation with flaring sources becomes available.

A general impression of the distribution of neutrino event arrival directions is given by maps of the sky shown in Fig. 13 (all events, i.e., mostly low energies), and Fig. 14 (highest energies, largest fraction of astrophysical neutrinos). In both cases, no obvious differences from the distribution expected for an isotropic incident flux are detectable. Nevertheless, more subtle analyses, a discussion of which we turn to now,

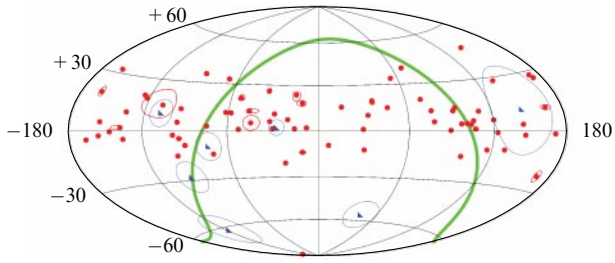

Figure 14. Distribution of IceCube event arrival directions with published energies above 200 TeV, Refs [17, 18, 21–24, 48] and GCN and AMON online alerts. Tracks are shown by dots, cascades are shown by triangles, lines indicate areas of 90% statistical uncertainty of arrival directions (not always distinguishable for tracks). About half of these events are atmospheric. Equatorial coordinates; Galactic plane is shown as a solid bold line.

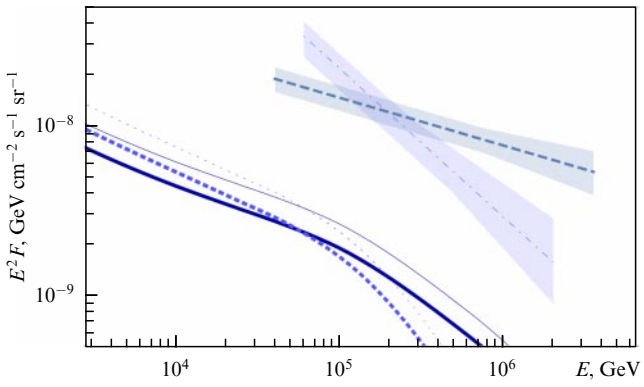

Figure 15. Neutrinos from the Galactic plane assuming proportionality of the flux to the predictions of the KRAγ model (in terms of one-flavor flux $\nu + \bar{\nu}$). Bold curves — best fit from IceCube cascade events [52], thin curves — strongest upper limits (90% CL) from a joint analysis of IceCube and ANTARES [51] (solid lines, KRAγ with cosmic-ray cutoff at 50 PeV, dotted, at 5 PeV). Lines with shaded uncertainty region show total astrophysical neutrino fluxes from IceCube data (blue dashed line — ν_μ 2019 [25]; thin blue dashed-dotted line — HESE 2020 [24]).

allow one to identify or constrain the contributions of various astrophysical sources.

2.3.1 Constraints on Galactic anisotropy. Neutrinos of extragalactic origin are collected from all over the Universe, so their flux must be isotropic to a high degree of accuracy. This distinguishes them from, for example, ultrahigh energy cosmic rays, whose mean free path length is hundreds of megaparsecs, so that their arrival directions could indicate a heterogeneous distribution of sources in that volume (for neutrinos, quantitative estimates of this effect are presented, e.g., in Ref. [49]). If, however, a significant fraction of the observed neutrinos are produced in our Galaxy, the inhomogeneities in the source distribution should show up in the anisotropy of the arrival directions. Unfortunately, with a significant background of atmospheric events it is difficult to search for such anisotropy; some interesting results have nevertheless been obtained.

Galactic plane. The distribution of visible matter in the Galaxy is far from isotropic — stars and gas are mostly contained in the disk visible in the sky as the Milky Way. For a quantitative answer to the question of what fraction of neutrinos may be associated with sources in the disk, the most effective way is to look for the 'Milky Way in neutrinos' against a background of uniformly (up to the experimental exposure) distributed atmospheric and extragalactic neutrinos. However, an ambiguity arises here, because the specific distribution of neutrino arrival directions from the disk depends on an assumption about the sources. Often, one uses the models constructed to explain the observed Fermi LAT direction- and energy-dependent intensity of Galactic diffuse gamma rays. Their free parameters include not only the distribution of matter and the magnetic field in the Galaxy but also the characteristics of the cosmic-ray flux. In particular, the spectrum and composition of cosmic particles, usually measured in the vicinity of the Sun, are extrapolated to the entire Galactic disk. Obviously, models of this type should be considered as estimates, and the scatter of their predictions for the neutrino flux demonstrates this systematic uncertainty. Recent observational results rely on the model of Ref. [50], called KRAγ, and consider two variants of it which assume the cosmic-ray spectrum cutoff at either 5 or 50 PeV (note that, in general, the results of cosmic-ray studies indicate their probable Galactic origin at higher energies as well).

In 2019, from an analysis of the anisotropy of IceCube cascade events [46], an indication was obtained (with the statistical significance of 2σ) of the presence of the Galactic component of the neutrino flux with the shape of the spectrum and the spatial distribution described by the KRAγ model, with the best-fit normalization of 0.85 (0.65) from the model prediction for cutoffs of 5 (50) PeV, respectively. The most stringent upper limits (coefficient of normalization of < 1.19 for the 5 PeV cutoff and < 0.90 for the 50 PeV cutoff, 90% CL) were obtained from a joint analysis of IceCube and ANTARES [51]. As can be seen from Fig. 15, if the detection of this component is confirmed, it would amount to $\sim 10\%$ of the IceCube astrophysical flux, in rough agreement with theoretical estimates. However, the mechanism of neutrino production in interactions of cosmic rays with the interstellar medium could not be unique for the Galactic disk; in particular, individual sources accelerating cosmic rays are present there. This analysis does not allow their contribution to be constrained. In this context, a nonparametric comparison of the observed and isotropic distributions of neutrinos at the Galactic latitude looks more universal. It allows us to find or constrain any flux component associated with the Galactic disk (see, e.g., [53, 54]).

Galactic center–anticenter. Another class of models, including those associated with dark-matter decays or annihilation and with the interactions of cosmic rays in the circumgalactic gas (see Section 4.2 below), predicts a different kind of Galactic anisotropy. In this case, the sources are not concentrated in the disk, but are distributed in the Galaxy in a more or less spherically symmetric way, with concentration decreasing from the Galactic Center to the virial radius, $\gtrsim 200$ kpc. Together with the noncentral position of the Sun in the Galaxy, this leads to a dipole-like anisotropy of arrival directions, with the maximum of the flux from the center of the Galaxy and the minimum from the opposite direction [55]. It is also convenient to search for such anisotropy, sensitive to the details of the source distribution, in the data with nonparametric tests [54]. Recently, experimental data analyses have used this approach in the context of particular dark-matter models [56, 57] together with the analysis of the

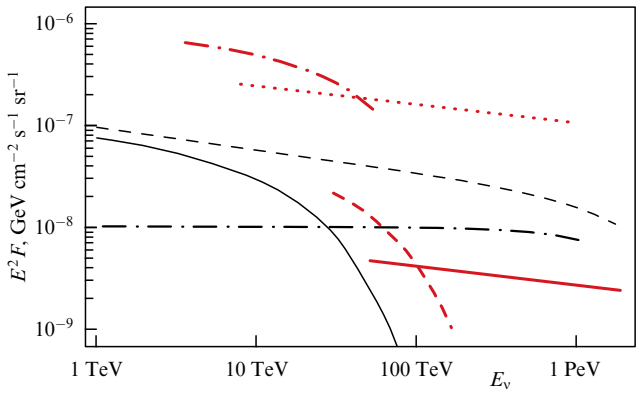

Figure 16. Constraints on models of neutrinos from Fermi bubbles. Bold red curves — upper limits on the neutrino flux ($\nu + \bar{\nu}$, one flavor, under the $E^{-2.18}$ spectrum assumption) from ANTARES [61] (dashed-dotted line — spectral cutoff at 50 TeV, dotted line — no cutoff) and IceCube [46] (dashed line — spectral cutoff at 50 TeV, solid line — no cutoff). Thin gray lines — proposed models (dashed — [62], dashed-dotted — lepto-hadronic [63], and solid — hadronic [63]).

contribution of dark matter to the observed neutrino spectrum [58, 59]. Increasing the sensitivity to particular models, these studies inevitably lose in universality. In most cases, adding a contribution with such anisotropy leads to an improvement in the description of the data, but this improvement is not statistically significant.

Large Galactic structures. The distribution of gas in the Galaxy and in the circumgalactic space is heterogeneous. In terms of the models of the neutrino origin discussed in the literature, so-called Fermi bubbles can be singled out: large-scale formations above and below the Galactic disk in its central region [60], possibly related to the past activity of the Galactic nucleus. Their contribution to neutrino fluxes can be constrained by treating them as extended sources, to which a higher flux of diffuse radiation in the sky map corresponds. The results of such analyses did not reveal any excess of neutrinos from the Fermi bubbles and allowed ruling out some models (Fig. 16).

A particular prediction of anisotropy also arises for the model of the Local Bubble (see Section 4.2), inside which we are located. The arrival directions of neutrino events in this model should concentrate in spots whose positions are determined by the direction of the Galactic magnetic field lines in the vicinity of the Sun. Because of great uncertainty in the knowledge of the Galactic magnetic field and of difficulties in quantitative analysis, the search for such anisotropy remains an interesting task for the future.

2.3.2 'Blind' search for point sources. Given the considerable uncertainty regarding theoretically motivated high-energy neutrino sources, the so-called blind search for their possible sources is becoming popular. Within this approach, the entire sky is searched for clusters of neutrinos coming from close directions that could indicate the most powerful point sources. The modern version implements this by constructing the maximum likelihood function, which takes into account not only the arrival directions but also the accuracy of their determination, which differs from event to event, as well as the energies: a cluster of even a few neutrino events allows one to estimate the hypothetical neutrino spectrum from a given direction, and if it is harder than the atmospheric one, then the probability that we are dealing with a real source and not with a background fluctuation is higher. Based on such maps, of which Fig. 13 is an example, many of the results of this and the next subsections have been obtained.

A significant disadvantage of the blind approach is that only the most powerful sources can be revealed in this way with high statistical significance. Indeed, in analyzing each individual direction, it is possible to determine the statistical probability that a cluster of events with all its characteristics arises as a result of a random fluctuation. To do this, it is sufficient to run a significant number of simulations of random sets of events and to calculate how often the observed, or larger, value of the likelihood function is reached due to fluctuations in these random sets. This probability [1] is the main characteristic of the significance of finding a hypothetical source. However, here we should distinguish between the probabilities of accidentally finding a 'source' (1) in a given predetermined direction and (2) anywhere in the sky. In the blind source search problem, we are dealing with case (2). The corresponding probability is much larger, which means that even a pronounced cluster of arrival directions can easily turn out to be random. If the probability of a random match for a given direction (pre-trial) is p_1, then, for N independent attempts, the probability (post-trial) becomes $p \sim Np_1$. If the assumption of independence of attempts is violated, p is determined from a Monte Carlo simulation. The ratio p/p_1, called the penalty factor (see, e.g., [64]), for a blind search for neutrino sources is easy to estimate approximately. Let us assume that the area of the uncertainty of the arrival direction of a track event is of the order of 2 square degrees, and half of the celestial sphere, that is, 2π steradian, is involved in the analysis. We then find the number of quasi-independent directions as the ratio of these areas, $\sim 10^4$ (a more correct estimate is required to take into account the anisotropy of the exposure). This means that, to assert the 3σ statistical significance of a source found in a blind search (i.e., $p \sim 10^{-3}$), one would need to have $p_1 \sim 10^{-7}$, that is, the pre-trial significance $> 5\sigma$.

The most significant blind search result for the dataset with the largest exposure, 10 years of IceCube track events, corresponds to the direction in the sky which is 0.35° away from the galaxy NGC 1068, a nearby galaxy with intense star formation. For this direction, $p_1 = 3.5\times10^{-7}$, $p = 9.9\times10^{-2}$, which corresponds to a post-trial significance of $\sim 1.6\sigma$. Additionally it should be noted that the fit indicates a very soft neutrino spectrum from this direction: the power-law index of the spectrum is 3.4, consistent with that expected for atmospheric, rather than astrophysical, neutrinos. Thus, at the time of writing this review, no individual source in the sky has been detected in a blind search with a post-trial significance exceeding even 2σ.

One way to increase the sensitivity of such an analysis to weaker sources is to use a priori fixed catalogs of theoretically justified neutrino sources. If the sources in the catalog are of one and the same type, then we are talking about a population analysis, and the cumulative signal from many, even weak, sources can be registered by summing multiple signals from their directions, each of which is statistically insignificant.

[1] For convenience, it is often recalculated into standard deviations for a normal distribution and is said to be significant at a certain amount of σ. Although we will also follow this tradition in this article, it is worth remembering that only the probability value itself is meaningful, since all involved distributions tend to be non-Gaussian.

This will be discussed in Section 2.3.3. Here, we mention recent attempts to increase the sensitivity of the blind search by combining different types of sources. A catalog of specific sources whose neutrino origins have been discussed in the literature is compiled and supplemented by sources somewhat similar to them. A wide variety of objects fall onto the same list. A blind search is limited to the directions of these 'justified' sources, and the penalty factor becomes equal to the number of sources in the catalog, i.e., instead of $\sim 10^4$, it becomes, for example, $\sim 10^2$. The danger of this approach is that some of the sources were actually 'justified' by previous analyses based on partial neutrino samples, which revealed excesses of neutrino events from their directions. Such an analysis can only make astrophysical sense if, along with an answer to the question of which sources the excesses of neutrino events are seen from, compared to random, there is also an answer as to why they are not seen from other similar sources.

Nevertheless, even along this path, no single source with a post-trial significance $> 3\sigma$ was found. Reference [65] analyzed a catalog of 110 gamma-ray sources identified from observational data in different bands, based on various criteria. This included 12 sources in the Galaxy, 3 nearby galaxies — the Large and Small Magellanic Clouds and the Andromeda galaxy — M31, 4 starburst galaxies, 89 active galactic nuclei, and 2 unidentified sources. All sources were studied as point sources, although the angular sizes of some Galactic sources, especially those of nearby galaxies, are noticeably larger than the IceCube angular resolution. For two sources, the post-trial significance was $> 2\sigma$; they are the already mentioned galaxy NGC 1068 and the blazar TXS 0506+056, which will be discussed in more detail in Section 2.3.4. Additionally, in Ref. [65], it has been observed that two other sources (blazars PKS 1424+240 and GB6 1542+6129) have pre-trial $p_1 < 2 \times 10^{-3}$ and that the presence of 4 sources out of ~ 100 with such low p_1, generally speaking, is in itself unlikely for a random fluctuation. The statistical analysis performed indicated the probability of such a coincidence at $\sim 5 \times 10^{-4}$ (significance $\sim 3.3\sigma$). This result, however, does not take into account the aforementioned arbitrariness in the compilation of the source catalog; in particular, the removal from it of TXS 0506+056, widely discussed previously, reduces the significance to 2.3σ [65]. The authors of Ref. [65] conclude from this analysis that the data indicate the presence of real sources in their catalog; however, an astrophysical interpretation of this result is difficult.

So far, we have mainly referred to the results of the search for neutrino sources in the Northern sky from IceCube track events. Similar work has been done for the Southern sky in the joint analysis of IceCube and ANTARES [66] and did not result in the detection of statistically significant individual sources either, including those in the region of the Galactic Center.

The lack of manifestations of significant individual sources in the analysis described in this section indicates that the observed flux of astrophysical neutrinos is produced by a large number of not very strong sources. This fact can be used to constrain the source models (see Section 3.2 below).

2.3.3 Source populations. The next natural step after a blind search is to take a population of the same type of astrophysical objects that are potential neutrino sources and check whether the entire population of objects has an excess of arrival directions compared to a random distribution. In this way, one can find or constrain the coherent effect from many sources of the same class, none of which is strong enough to be detected statistically significantly in an individual or blind analysis. Technically, such an analysis can be performed either using the likelihood function described in Section 2.3.2 (test statistics are based on the sum of the values of the likelihood function for all directions from the sources in the catalog) or by counting the number of sources from the catalog in the area near each neutrino arrival direction (in this case, the test statistics are simply the total number of 'source–neutrino pairs'). In both cases, a weight can be assigned to each source, e.g., depending on the flux of its electromagnetic radiation in a particular band or from other considerations. In the second approach, the size and the shape of the region are given by the accuracy of determining the neutrino arrival direction (e.g., at the 90% CL). These approaches have their pros and cons: the likelihood function allows one to account for 10% of events that fall outside the 90% CL angular resolution, and may contain additional information, encoded in continuous characteristics of events, such as energy, influencing the probability that a given neutrino is astrophysical. At the same time, when counting events, it is easier to account for a poorly known systematic error in determining the arrival direction of neutrinos, discussed in Section 1.2 (see, e.g., [67, 68]). Typically, the likelihood function is used for large numbers of neutrino events (low energies) or for extended uncertainty regions of complex shape (cascades).

Table 4 provides a summary of numerous (but perhaps not all) published analyses of correlations of neutrino arrival directions with potential source populations. As one can see, there are only a few statistically significant results. The first fact that draws attention is the lack of correlations with gamma-ray bright blazars from the Fermi LAT catalogs, which, before the detailed analysis of IceCube results, were considered to be among the most likely sources of high-energy neutrinos. That said, a few statistically significant results point to blazars selected according to other criteria. Let us briefly discuss them.

By definition, a blazar is the nucleus of an active galaxy that has a relativistic jet pointing almost exactly at the observer. Relativistic kinematic effects lead in this case to strong amplification of the observed radiation flux. The same mechanism of amplification works for neutrinos. Physical conditions in nuclei and jets allow protons to be accelerated to the energies required for neutrino production. All of this together makes blazars very attractive candidates for high-energy neutrino sources.

While identification as a blazar is determined only by this geometric characteristic of the jet, physical conditions in these sources may be different. They are manifested primarily in which bands the blazar emits the dominant part of its nonthermal radiation. The main characteristic here is the frequency, corresponding to the maximum of the synchrotron peak in the broadband spectral energy distribution, which varies from $\nu_{\rm peak} < 10^{12}$ Hz (radio band — radio quasars with a flat spectrum, FSRQ) to $\nu_{\rm peak} > 10^{17}$ Hz (X-ray band — extreme BL Lac type objects, HBL). In many studies, the primary focus has been on blazars bright in the gamma-ray band, observed by Fermi LAT (1–100 GeV). These are the highest energies at which samples of sources fairly uniform over the sky are available; in addition, at even higher energies, the Universe becomes not completely transparent to gamma rays because of e^+e^- pair production (see Section 3.1).

Table 4. Results of searches for correlations of high-energy neutrino arrival directions with populations of astrophysical sources. Source selections: all Galactic sources are selected from observations above 100 GeV; for the selection of other gamma-ray sources, Fermi LAT catalogs were used: all sources, 3FGL [73]; sources detected above 50 GeV, 2FHL [74], and above 10 GeV, 3FHL [75]; gamma-ray bright active galactic nuclei (AGN), 3LAC [76] and 4LAC [77], and the VOU-blazars database [78]. Nongamma-ray related selection criteria for blazars included a high-frequency ($> 10^{15}$ Hz, HBL) synchrotron peak, 2WHSP [79] and 3HSP [80] catalogs, and the presence of a compact core visible with very-long baseline radio interferometers, RFC catalog (http://astrogeo.org/rfc). Selection of neutrinos: based on the data from IceCube (I) or ANTARES (A), ν_μ — only track events, number in parentheses — number of years of exposure, HE — published individual high energy events, 200+ — energies above 200 TeV. Method: L — likelihood function, C — coincidence counting. Post-trial significance: not specified if less than 2.5σ. Contribution to the flux: estimate of the fraction of the astrophysical flux assuming a power-law fit for tracks (ν_μ) or cascades ($\nu_{e,\tau}$) associated with the sources of a given sample.

Source sample	Number of sources	Neutrino sample	Method	Reference	Post-trial significance	Contribution to flux
Galactic sources						
Supernova remnants	23	I ν_μ (10)	L	[65]	—	
Pulsar wind nebulae	33	I ν_μ (10)	L	[65]	—	
Pulsar wind nebulae	35	I ν_μ (9.5)	L	[69]	—	$< 48\%$ ν_μ
Unidentified gamma-ray sources > 100 GeV	23	I ν_μ (10)	L	[65]	—	
Extragalactic sources other than blazars						
Starburst galaxies	45	I ν_μ (3)	L	[70]	—	
Starburst galaxies	64	A (10)	L	[71]	—	
Radio galaxies	63	A (10)	L	[71]	—	
Dust-obscured galaxies	15	A (10)	L	[71]	—	
Gamma-bright (4LAC) AGN other than blazars	65	I ν_μ (3)	L	[70]	—	
Large-scale extra-galactic jets	94	I HE all	C	[72]	—	
Gamma selected blazars						
3FGL	729	I ν_μ 200+	C	[81]	—	
2FHL BL Lacs		I ν_μ 200+	C	[82]	—	
2FHL HBL	149	I ν_μ (7)	L	[48]	—	$< 27\%$ ν_μ
2FHL HBL	149	I HE all	C	[83]	—	
3FHL	1301	I ν_μ (8)	L	[84]	—	$< 17\%$ ν_μ
3FHL	1301	I HE ν_μ	C	[68]	—	
3LAC HBL	386	I HE ν_μ	C	[83]	—	
3LAC	1255	A (10)	L	[71]	—	
3LAC FSRQ	414	I ν_μ (7)	L	[48]	—	
4LAC	2796	I ν_μ (3)	L	[70]	—	$\lesssim 11\%$ $\nu_{e,\tau}$
4LAC	2794	I HE ν_μ	C	[68]	—	
VOUγ HBL		I HE ν_μ	C	[68]	3.2σ	$\sim 21\%$ ν_μ
Blazars selected by other criteria						
2WHSP	1681	I ν_μ (7)	L	[48]	—	
2WHSP	1681	I HE all	C	[83]	—	
3HSP	2011	I HE ν_μ	C	[68]	2.8σ	
RFC	3388	I ν_μ 200+	C	[67]	3.1σ / 3.0σ } 4.1σ	
RFC	341	I ν_μ (7)	L	[85]		$\sim 25\%$ ν_μ
RFC	3388	I ν_μ (10)	L	[86]	—	$\lesssim 30\%$ ν_μ

Unfortunately, due to the insufficient sensitivity of Fermi LAT and the strong variability of blazars in the gamma-ray band, samples of gamma-ray bright sources capture only a small fraction of blazars. It is also possible that this fraction is unrepresentative, because the origin of gamma rays in different classes of blazars can be very different. The

universal criterion for the presence of a relativistic jet directed towards us is the observation of a compact (no more than a few parsecs in size) region of intense radiation at the center of the source, located at a gigaparsec-scale distance [87, 88]. For this, one requires an angular resolution achievable in modern astronomy only with very-long baseline radio interferometry (VLBI) [89]. A catalog of such compact, VLBI-selected, objects, the Radio Fundamental Catalog (RFC), is the basis for the search for neutrino arrival direction coincidences with blazars in Refs [67, 85]. Specifically, a complete sample, limited in the compact-component flux at 8 GHz, of about 3400 blazars isotropically distributed over the celestial sphere was used.

Reference [67] analyzed a sample of 56 arrival directions of published IceCube track events with neutrino energies $E_\nu > 200$ TeV. The VLBI flux of complete-sample sources near the neutrino arrival directions (more precisely, in the 90% CL regions of statistical uncertainty of the arrival directions plus the systematic uncertainty estimated in the analysis) was used as the test statistics. This average flux turned out to be significantly higher than expected for the random distribution of arrival directions of neutrino events. After accounting for the penalty factors associated with variation in the amount of systematic error, the statistical significance of the established relationship between VLBI sources and high-energy neutrinos was found to be 3.0σ. Additionally, Refs [67, 90] found the coincidence of neutrino arrival times with radio flares of these correlated blazars (see Section 2.3.4).

In the spring of 2020, the IceCube collaboration published the values of the likelihood function described in Section 2.3.2, constructed from seven years of track-event observations (this is the one presented in Fig. 13). In Ref. [85], based on these data (for directions from below the horizon, where the flux of atmospheric muons is strongly suppressed), a correlation of directions with the maximum probability of locating a point source of astrophysical neutrinos with directions to blazars from the same RFC catalog was established (significance of 3.1σ post trial). The joint statistical significance of the observations [67] and [85] was estimated, as they were based on the same sample of sources. To make the two analyses completely independent, directions of neutrinos with energies above 200 TeV, used in analysis [67] and recorded during the time period for which the likelihood map was constructed, were cut from the map. The cumulative statistical significance of neutrino correlations with the VLBI-selected blazars was found to be 4.1σ. The data underlying the likelihood function were dominated by events with energies from a few TeV to several tens of TeV, and the unexpected result of this analysis was the association of neutrinos of the entire range of energies studied by IceCube, from TeV to PeV, with sources of the same class. The sources in the complete sample included in the analysis are responsible for about 25% of the astrophysical flux estimated from muon tracks (assuming power law (4) with parameters [25] over the entire energy range). Taking into account the correction for similar sources not present in the catalog raises this value to $\sim 100\%$.

It should be noted that, in Ref. [86], the same set of VLBI-bright blazars was used for a correlation analysis with the recently published 10-year IceCube public dataset of muon tracks [19, 20]. Despite the increased exposure (compared to the 7-year set [46, 47] used in Ref. [85]), this analysis found no significant correlations. The contribution of blazars from the catalog to the flux of astrophysical neutrinos was limited to $\lesssim 30\%$, which is consistent with the result of Ref. [85] ($\sim 25\%$). Note that this IceCube dataset is not well suited to test the hypotheses formulated earlier, since it contains neither the likelihood function nor reconstructed energies of individual neutrinos (only muon energies E_μ (see Section 1.2 and Fig. 1) are published). The authors of Ref. [86] constructed their own likelihood function, simplified compared to the IceCube function used in [85], which took into account the neutrino energies. The sensitivity of such an analysis is low, so it is not surprising that it neither confirmed nor ruled out the result of Ref. [85]. The work to test the hypothesis of a connection of neutrinos with VLBI-bright blazars continues with the data from Northern hemisphere experiments. Preliminary results [91] of the ANTARES collaboration indicate the presence of a correlation of arrival directions, compatible with that found from IceCube [85].

Correlations (significance 3.2σ post trial) of the arrival directions of IceCube high-energy track events published as separate lists and alerts, with blazars selected on the basis of other criteria, have been found in Ref. [68]. The sample of sources used there was not complete by any criterion, but was a combination of heterogeneous data based on observations in different bands. The only requirement was the registration of gamma rays from the blazar by some instrument. Forty-eight coincidences of directions of arrival of neutrinos to the blazars were found, with an expectation of ~ 32 for random directions. It is interesting to note that 39 of these 48 blazars are present in the RFC catalog, that is, they have a VLBI-compact component, indicating the presence of parsec-scale relativistic jets, and 16 of them belong to the complete sample used in Refs [67, 85]. Therefore, the effect found in Ref. [68] is actually saturated by sources of the same class.

Thus, blazars, that is, active galaxies with relativistic jets pointing almost exactly toward the observer (but not necessarily bright in the gamma-ray band investigated by Fermi LAT), given the contribution of sources not listed in the catalogs, can explain the entire astrophysical neutrino flux, as estimated from IceCube muon tracks, when extrapolated to energies of the order of TeV by a power law (4). In the context of the two-component model discussed in Section 2.2, this corresponds to 100% of the hard flux component.

2.3.4 Search for flares. A blind search for neutrino flares from arbitrary directions in the sky opens up even more freedom in the parameters — time and duration of the flare are added to the direction in the celestial sphere. The probability of finding a spatiotemporal cluster of events resulting from random fluctuations is very high, and studies of this kind in the presence of a large random background make sense only for predetermined sources, whose variability in electromagnetic radiation could be associated with neutrino bursts. The most highly variable objects among potential neutrino sources are blazars and one-time catastrophic events on stellar scales (see, e.g., Ref. [92]). Neutrino flares are often searched for in spatiotemporal coincidence with such events or with flares of electromagnetic radiation from blazars. Note that often 'neutrino flare' means the moment of arrival of a single rare (high-energy) event with a high probability of astrophysical origin. However, these results should be interpreted with caution: for the Poisson statistics, a single event may signal both an increase in the average expected rate of arrival of events (a flare) or a completely random single event at an expected rate of less than one event during the observation

time. The estimation of the neutrino flux in this case is ambiguous [93].

AMANDA and 1ES 1959 + 650. Historically, the first claim of a coincidence of neutrino and gamma-ray flares of a blazar was made by the AMANDA collaboration based on 2002 data [94, 95]. From the direction of the blazar 1ES 1959 + 650, over 4 years of observations, 5 neutrino events were observed at an expectation of 3.7, which by itself is consistent with fluctuations. However, 3 of these 5 events came in a time interval of 66 days, coinciding with flares of this source in TeV gamma rays. The collaboration refrained from assessing the statistical significance of this coincidence, because it was detected *a posteriori*, not in a 'blind' analysis. Theoretical interpretations of this observation were controversial [96, 97]. New similar gamma-ray flares of the same blazar in 2016 were not accompanied by neutrino excesses at IceCube; this, however, does not contradict the predictions of the proposed models [98]. It was this observation by AMANDA which motivated the development of a system of mutual neutrino and gamma-ray telescope alerts [4], which has been actively developing already in the IceCube era.

IceCube and TXS 0506 + 056. One of the most widely known cases of a coincidence of a detected IceCube neutrino event with a gamma-ray blazar flare is the neutrino alert IC170922A, associated with the blazar TXS 0506 + 056. Unlike its AMANDA predecessors, the IceCube collaboration in this case, quite similar to the one described above, has evaluated and published [15] *a posteriori* the statistical significance of this coincidence. In describing this well-known event, we follow the original study [15].

A muon track, corresponding to a high probability to an astrophysical neutrino with an energy of hundreds of TeV (an estimate of the energy of this event is shown in detail in Fig. 1), was recorded on September 22, 2017. A standard analysis demonstrated a coincidence of the arrival direction with the position of the gamma-ray bright blazar TXS 0506 + 056, which was in a period of increased activity. In response to an IceCube alert, this source was observed by atmospheric Cherenkov telescopes recording gamma rays with energies $\gtrsim 100$ TeV: on September 23, by HESS and VERITAS and on September 24, by MAGIC. Gamma rays from this source were not detected by the three instruments; however, when MAGIC repeated its observation on September 28, it detected a nonzero signal corresponding to an increase in the flux in comparison with the upper limits from September 23–24. Multi-wavelength observations demonstrated that, at the time of the neutrino arrival, the blazar was at the beginning of a prolonged flare in the radio band; its X-ray flux was quite modest (this observation has severely limited theoretical models of the neutrino origin). In the optical band, a few minutes after neutrino detection, a strange short drop in the brightness of the source was observed [99].

Blazars are numerous and highly variable sources, so the probability of accidentally finding one in a flaring state in a given direction and at a given moment in time is quite high. In the absence of an a priori fixed procedure, a correct estimate of the probability of such a coincidence is difficult: the main problem is to choose what to call a 'flare' of the source and what to call a 'coincidence' with the flare. The authors of Ref. [15] proposed and applied several methods for assessing the statistical significance, described in the Supplementary Information to their paper. For these estimates, only correlations with Fermi LAT were used, since only this instrument provides continuous observations of blazars across the entire sky to which a particular detected flare can be compared. The probability of a random coincidence, calculated *a posteriori* and not accounting for different trials, was 2.1×10^{-5} (4.1σ pre-trial). The authors of the paper counted observations of other neutrino events (at the time of the event analysis, there were a total of 51 events selected using the same criteria as IC170922A) for which there was no overlap with gamma-ray bright blazar outbursts as independent trials. Taking into account the corresponding penalty factor results in the probability $\approx 10^{-3}$ (3.0σ post-trial). This estimate does not account for the additional penalty factor for testing four models of gamma-flux correlation, three of which can be considered independent, or for the choice of the Fermi LAT light curve simulation parameters (bin size in time and the choice of the energy bin). Note also that, after the publication of this result, IceCube changed the criteria for selecting alert events, so that a statistically correct analysis of how many other similar neutrino events were not accompanied by flare gamma-ray sources since then is not possible.

From the facts that only for one gamma-ray source has such a coincidence been reported and that population analyses do not indicate a significant association of gamma-ray bright blazars with neutrinos (see Section 2.3.3), it has been suggested that the blazar TXS 0506 + 056 is a 'special' source, so the history of detection of neutrinos of all energies from this direction was analyzed. A flare of neutrino events (19 events with an expectation of 6) with energies of 0.1–20 TeV and a significance of 3.5σ (post-trial) was found in [100] from that specific direction in the sky. The time period in which this neutrino flare happened, 2014, was not special in terms of the gamma-ray activity of the source [101]. Note that, using the IceCube event reconstruction published in 2021 [19, 20], the pre-trial probability of registering this flare as a result of random fluctuations is only 8.1×10^{-3} [19], which is ~ 100 times higher than in the original analysis. With the same change in the post-trial significance, it would amount to $\approx 2\sigma$.

Numerous papers have investigated multiwavelength characteristics of this source in order to give a theoretical description of neutrino production (see, e.g., [102–111]). It was not possible to propose a model that simultaneously describes the events of 2014 and 2017 within a single mechanism. A study of the characteristics of the TXS 0506 + 056 source demonstrated that it is a typical radio blazar [112]. Thus, the observations [15, 100] may not testify to the singularity of this source, but serve to illustrate the established population connection of neutrinos and radio blazars [67, 85]; the gamma-ray flare might be only a simultaneous signal of the source activity.

Flares of radio blazars. This interpretation motivated the search for coincidence of arrival moments of high-energy IceCube neutrinos with radio flares of the blazars [67] located in the same directions. The result of this study is illustrated in Fig. 17, from which one can see that, on average, the blazars coinciding with the neutrino arrival directions are in the period of the radio flare at the time of neutrino arrival. Despite the impressive appearance of the figure, the post-trial statistical significance of this result is only slightly greater than 2σ due to the penalty factor for the selection of the optimal time-window size. This result, obtained with the data of the blazar monitoring program with the RATAN-600

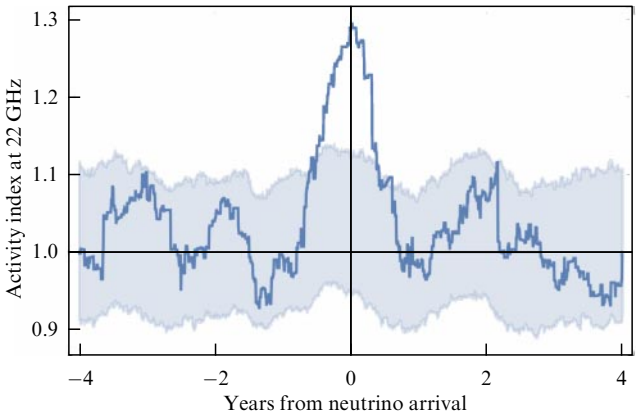

Figure 17. Coincidence of arrival moments of $E_\nu > 200$ TeV neutrinos with flares of blazars selected from the VLBI catalog (22 GHz RATAN-600 data from Ref. [67]). Activity index is defined as the ratio of radio flux in the optimized period of 0.9 year to flux for the entire period of observations. Averaged over 18 sources coinciding with neutrino arrival directions. Shaded area is the expectation for random arrival directions (68% CL).

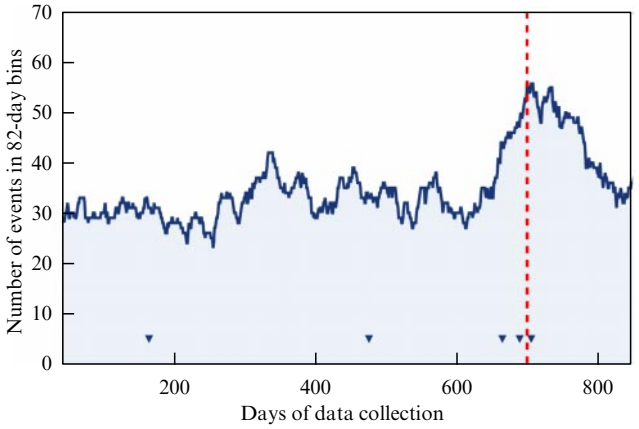

Figure 18. Count rate of events with estimated primary energy above 300 TeV from the direction of the Cygnus Cocoon, as recorded by the Carpet-2 facility. Vertical dashed line indicates the arrival time of a neutrino with energy ~ 154 TeV from this direction. Inverted triangles at the bottom of the figure indicate the arrival times of the events that have been most rigorously filtered out as candidates for primary photons. Plotted with data from Ref. [134].

telescope (Special Astrophysical Observatory of the Russian Academy of Sciences), was confirmed by observations of the American OVRO and Finnish Metsahovi observatories [90].

Cosmic gamma-ray bursts. These stellar-scale processes with extreme energy release [113–115] have long been considered as potential sources of high-energy protons and neutrinos (see, e.g., [116–119]), but no space-time correlation between neutrinos and detected gamma-ray bursts has been found [120–123]. This narrows the range of gamma-ray bursts — potential sources of high-energy neutrinos — to optically thick ones not observed in electromagnetic radiation, for which such an analysis is not possible.

Tidal disruption of stars. These catastrophes occur when a star collides with a black hole and are observed primarily as flares in the optical band. Rarely, these events are accompanied by the formation of a jet. The absence of spatiotemporal correlations with the population of such sources limits their contribution to the IceCube astrophysical neutrino flux to the level of $\lesssim 1\%$ (for processes with jet formation, $\lesssim 26\%$) [124]. There has been some interest in the IceCube neutrino event IC191001A with an energy of ~ 217 TeV, which coincided in arrival direction with one of the tidal disruption events, AT2019dsg, although the neutrino came 154 days after it [125]. The authors of that paper give only an estimate of the probability of a random coincidence, $\approx 4.8 \times 10^{-3}$, without a detailed statistical analysis. This coincidence is discussed in more detail in Ref. [126]. Note that, in this case, the tidal disruption of the star was not accompanied by the formation of a jet.

Galactic sources. As discussed below in Section 3.1, for sources in our Galaxy, it is possible to observe high-energy neutrinos along with associated gamma rays of the same energy range. Gamma-ray astronomy above 100 TeV is now being intensively developed, motivated in large part by the neutrino results of IceCube. The observations of point sources [127–132] and of diffuse gamma rays from the Galactic plane [133] in this band are worth mentioning. So far, the only indication of a possible connection between a flare of gamma rays with energies above 100 TeV from a Galactic source and neutrinos of the same energy comes from the Carpet-2 facility (Baksan Neutrino Observatory, INR RAS), which has recorded an increased flux [134], coinciding with the arrival time of a neutrino with an energy of ~ 154 TeV, from the region of the Galactic disk in the Cygnus constellation, which includes the so-called Cygnus Cocoon, a probable source of the most energetic cosmic photon ever recorded (1.4 PeV [132]). In Fig. 18, the dependence of the rate of arrival of atmospheric showers from the direction of this source is shown. The observed excess corresponds to a flare of photons with energies $\gtrsim 300$ TeV lasting about 3 months around the day of the neutrino event. The statistical significance of this flare is 3.1σ (post-trial). Note that, although it is the Cygnus Cocoon that coincides with the most likely direction of neutrino arrival, both the accuracy of this direction and the angular resolution of Carpet-2 are worse than 4°, and other interesting sources are present in this uncertainty region, including relativistic binary systems detected in gamma rays above 100 GeV.

3. General constraints on models of neutrino origin

3.1 π-meson mechanism and the multimessenger approach

Neutrinos have no electric charge and therefore cannot be efficiently accelerated by external fields. Thus, high-energy neutrinos can only be produced in decays or interactions of other energetic or heavy particles. Examples of these processes are decays of ultrarelativistic nuclei (we will mention this mechanism at the end of this section) and decays or annihilation of very heavy slow particles (dark matter; see Section 4.2). However, the most natural mechanism, guaranteed under astrophysical conditions, is associated with the decays of π-mesons born in the interactions of cosmic rays with matter or radiation.

Indeed, experiments indicate the presence in our Galaxy (and probably in other galaxies as well!) of high-energy hadrons — cosmic-ray particles, protons, and nuclei [45,

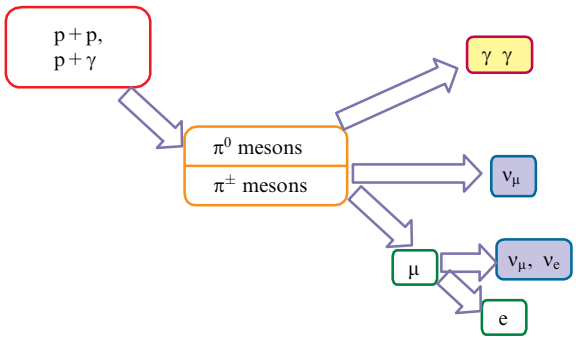

Figure 19. Basic processes of neutrino production in astrophysical sources [14].

135]. These particles interact with surrounding matter and radiation. At high energies, most of the interactions involving hadrons results in the production of the lightest of the strongly interacting particles, π mesons; they are unstable and their decay products include high-energy neutrinos. These processes must take place wherever there are high-energy hadrons (cosmic rays), but their intensity depends on the amount of matter in the medium or of the target photons.

Proton–proton interactions. Without loss of generality, we will assume that both relativistic hadrons and ambient hadrons are protons (p). At high energies, pp-interactions proceed with the birth of one or more π mesons [136–138], with the leading π meson carrying away on average $\sim 1/5$ of the energy of the relativistic proton, E_p, in the rest frame of the target proton. The birth of π^0, π^+, and π^- mesons is approximately equally probable, and high-energy emission is determined by the decays (Fig. 19)

$$\pi^0 \to \gamma\gamma\,, \tag{5}$$

$$\pi^+ \to \mu^+\nu_\mu\,, \tag{6}$$

$$\mu^+ \to \mathrm{e}^+\nu_\mathrm{e}\bar{\nu}_\mu \tag{7}$$

(the decay chain of π^- and μ^- is obtained from Eqns (6) and (7) by charge conjugation). The energy of a charged π meson is divided, on average about equally, among the four leptons in the final state, or more precisely [1, 139]

$$\frac{\langle E_{\nu_\mu}\rangle}{E_{\pi^+}} = \frac{1}{2}\left(1 - \left(\frac{m_\mu}{m_\pi}\right)^2\right) \simeq 0.21\,,$$

$$\frac{\langle E_{\nu_\mathrm{e}}\rangle}{E_{\pi^+}} = \frac{1}{10}\left(2 + \left(\frac{m_\mu}{m_\pi}\right)^2\right) \simeq 0.26\,,$$

$$\frac{\langle E_{\bar{\nu}_\mu}\rangle}{E_{\pi^+}} = \frac{\langle E_{\mathrm{e}_+}\rangle}{E_{\pi^+}} = \frac{1}{20}\left(3 + 4\left(\frac{m_\mu}{m_\pi}\right)^2\right) \simeq 0.27\,.$$

The energy of the neutral π meson is divided equally between the two produced photons. Thus, as a result of the interaction of a proton with E_p with a proton at rest, on average, either two photons with energies of $E_\mathrm{p}/10$ each, or (with the probability of 2/3) three (anti)neutrinos with energies of $E_\mathrm{p}/20$ are produced.

Proton–photon interactions. Consider now the interaction of relativistic protons with photons of the ambient radiation. At extremely high energies, this process also takes place with multiple π-meson production, and in terms of the resulting neutrinos is not much different from the pp-interaction. However, we are more interested in the other regime. Indeed, significant concentrations of photons in astrophysical sources are reached only at relatively low energies, so the main contribution to the production of astrophysical neutrinos comes from interactions with single π-meson production. Unlike for pp, the production of π mesons in pγ interactions is a threshold process, and the total energy must be sufficient to produce at least a π meson at rest. The main channel for this is the resonant birth and subsequent decay of the Δ^+ baryon,

$$\mathrm{p} + \gamma \to \Delta^+ \to \begin{cases} \mathrm{n} + \pi^+\,, \\ \mathrm{p} + \pi^0 \end{cases} \tag{8}$$

(n denotes a neutron).

The first thing that draws our attention is that, in this process, no leading π^- is produced, so the equality of ν_e and $\bar{\nu}_\mathrm{e}$ at birth is violated. However, for the sum of neutrinos and antineutrinos, the flavor content obtained in pγ-interactions does not differ from the pp case.

Further, the kinematics of two-particle decay Δ^+ allows us to determine the fraction of the energy of the initial particles carried away by the π meson: it is again $\sim 1/5$ (the numerical agreement with the pp case is accidental and takes place only in the Δ-resonance approximation), so, as with the pp-process, $E_\nu \sim E_\mathrm{p}/20$ and $E_\gamma \sim E_\mathrm{p}/10$ (but, due to the absence of π^-, photons are now born in about 1/2 of cases rather than 1/3).

Finally, the resonance condition will be written as $E_\mathrm{p}E_{\gamma_\mathrm{B}} = m_\Delta^2$, where E_{γ_B} is the energy of the initial photon, and $m_\Delta \approx 1.23$ GeV is the Δ baryon mass. Therefore, for the production of a neutrino with energy E_ν in the pγ process, we can estimate the required energy not only for the proton, $E_\mathrm{p} \simeq 20E_\nu$, but also for the initial photon,

$$E_{\gamma_\mathrm{B}} = \frac{m_\Delta^2}{20E_\nu} \simeq 750\ \mathrm{eV}\left(\frac{E_\nu}{100\ \mathrm{TeV}}\right)^{-1}. \tag{9}$$

For practical applications, it is important to remember that Eqn (9) is written in the source frame, so E_ν here may be different from the observed one, e.g., if the source is located at a cosmological redshift z or if the source is moving relativistically along the line of sight. Note also that the estimates given here and in the description of the pp-process are easily memorized but approximate and in a number of cases do not work (see, e.g., [140]).

In many models of acceleration of cosmic-ray particles, the spectrum of relativistic protons turns out to be power-like. For scattering on protons at rest, the scale invariance of the pp-process leads to the fact that the spectra of secondary particles and, eventually, neutrinos repeat the power-law spectrum of the original protons. The resonant nature of pγ-scattering, in contrast, leads to neutrino spectra that are different from the power law and are determined by the spectra of target photons.

Oscillations and flavor content. So, from the decays of $\pi^\pm$ mesons, one obtains ν_e, ν_μ, and corresponding antineutrinos. In pp-interactions, neutrinos and antineutrinos are born equally, while in the pγ case the production of $\bar{\nu}_\mathrm{e}$ is suppressed in the Δ-resonance approximation. In either case, twice as many muon neutrinos and antineutrinos are

produced in total than electron ones. However, on the way from the source to the observer, the flavor composition of the neutrinos changes due to oscillations.

Let us denote the difference in the squared masses of the two neutrino states as Δm^2, and the neutrino energy as E_ν. Then, the oscillation length is

$$L_{\rm osc} = 4\pi \frac{E_\nu}{\Delta m^2} \approx 22.4 \text{ au} \left(\frac{E_\nu}{100 \text{ TeV}}\right) \times \left(\frac{\Delta m^2}{7.4 \times 10^{-5} \text{ eV}^2}\right)^{-1}. \quad (10)$$

Given that the radius of the orbit of Uranus is about 19 au, we derive that the distance to any neutrino source outside the Solar System is much larger than the oscillation length (to estimate this, the smallest Δm^2 in the system of three neutrino flavors was substituted into Eqn (10)). In addition, for most astrophysical sources, their size is also noticeably larger than $L_{\rm osc}$. Therefore, for the flavor composition of neutrinos at detection, it makes sense to consider only the average over the oscillation phases, which means that the so-called Gribov–Pontecorvo approximation works. Within this approximation, the fractions of neutrinos of flavors $l = \text{e}, \mu, \tau$ at the observation point, f_l, are related to those at the source, $f_l{}^0$, by the simple relation

$$f_l = \sum_{l'} M_{ll'} f_{l'}^0 , \quad (11)$$

where the transformation matrix $M_{ll'} = \sum_i |U_{li}^2||U_{l'i}^2|$, and U_{li} is the neutrino mixing matrix (the Pontecorvo–Maki–Nakagawa–Sakata matrix; see, e.g., [141]). The values of elements of this matrix, the neutrino oscillation parameters, are known with a certain accuracy and continue to be refined in new experiments (see Ref. [142]). For the purposes of this review, an approximation in which $f_\tau^0 = 0$ is sufficient; then, $f_\mu^0 = 1 - f_{\rm e}^0$ and

$$\begin{cases} f_{\rm e} \simeq 0.18 + 0.36 f_{\rm e}^0 , \\ f_\mu \simeq 0.44 - 0.25 f_{\rm e}^0 , \\ f_\tau \simeq 0.38 - 0.11 f_{\rm e}^0 . \end{cases} \quad (12)$$

Notably, for the value $f_{\rm e}^0 \approx 1/3$ expected from π-meson decays in the source, we obtain an approximate equality of the detection probabilities of the three neutrino flavors at the detection point.[2]

The multimessenger approach. Since low-energy photons and target protons are abundant in many astrophysical objects, the mechanism described above links fluxes of three types of high-energy particles, the astrophysical messengers: neutrinos from $\pi^\pm$ decays, photons from decays of π^0, and the original relativistic protons, cosmic rays. This link underlies the so-called multimessenger approach to observational constraints on source models. Constraints of this type had been used to estimate high energy astrophysical neutrino fluxes for decades before their discovery [143–145], and after the discovery they became a powerful quantitative tool to understand the neutrino origin.

[2] Expression (11) is valid for both neutrinos and antineutrinos. Given that, with the exception of the Glashow resonance, it is impossible to distinguish ν and $\bar{\nu}$ by modern experiments, we do not distinguish between them in these expressions.

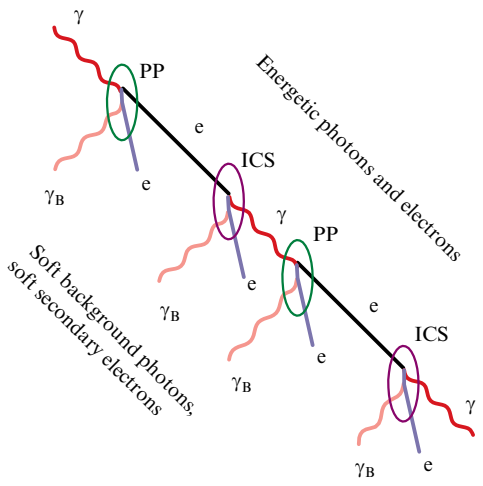

Figure 20. Electromagnetic cascade development [14]. PP — pair production, ICS — inverse Compton scattering.

We have seen that in π-meson decays the emitted flux of neutrinos of energies E_ν is accompanied by an emitted flux of photons at energies $E_\gamma \sim 2E_\nu$. The energy fluxes (measured, for example, in TeV cm^{-2} s^{-1}) carried away by photons γ and neutrinos ν are related as

$$E_\gamma^2 \frac{{\rm d}N_\gamma}{{\rm d}E_\gamma} = A E_\nu^2 \frac{{\rm d}N_\nu}{{\rm d}E_\nu}\bigg|_{E_\nu = E_\gamma/2},$$

where $A \sim 2/3$ (4/3) for the pp (pγ) mechanism, respectively. However, unlike neutrinos, high-energy photons do not propagate through the Universe freely: they produce electron–positron pairs e^+e^- in interactions with photons of the background radiation [146]. This process is a threshold one, and its cross section peaks strongly just above the threshold, when the energies of the initial photons satisfy the ratio $E_\gamma E_{\gamma_{\rm B}} \approx 4m_{\rm e}^2$, where $m_{\rm e}$ is the mass of an electron. It is convenient to rewrite this relation in the form

$$\frac{E_\gamma}{\text{TeV}} \frac{E_{\gamma_{\rm B}}}{\text{eV}} \approx 1 , \quad (13)$$

from which it follows that photons with $E_\gamma \sim 100-1000$ TeV produce pairs mostly on cosmic microwave background photons, whose density in the Universe is very high. As a consequence, the mean free path of photons born jointly with neutrinos does not exceed the size of the Galaxy or its immediate vicinity. This, however, is only part of the story, since the produced $\text{e}^\pm$ interact with the same background radiation, transferring their energy to photons (inverse Compton scattering). The resulting photons, each with energy already slightly lower than that of the initial one, again produce electron–positron pairs, and the electromagnetic cascade continues (Fig. 20). After each cycle, the energy of the original photon is redistributed among secondary photons, so that the average energy of the photons in the cascade decreases, although the total energy is conserved (see Refs [144, 147]). This continues until the average energy of the photons drops so much that they continue moving through the Universe unimpeded. This occurs at photon energies of several tens of GeV, so that all the energy of extragalactic diffuse gamma rays with $E_\gamma \gtrsim 100$ TeV is 'pumped' into the ~ 10 GeV range. The flux of isotropic gamma rays in this range has been measured by the LAT instrument [148] aboard

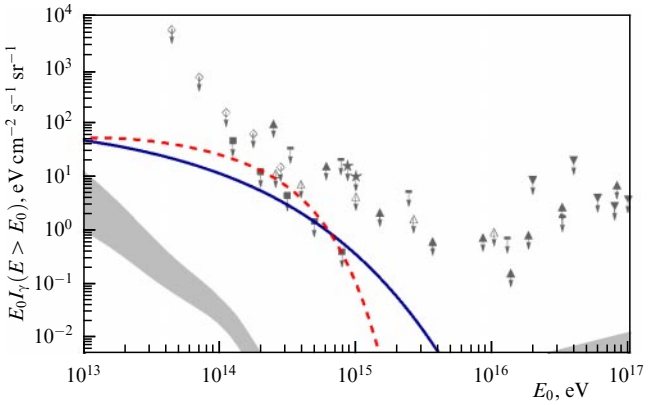

Figure 21. Predictions of the integral isotropic diffuse flux of high-energy photons in models explaining the observed neutrino flux: Galactic (solid line — interaction of cosmic rays with gas in the walls of the Local Bubble [149], dashed line — dark-matter particle decays [150]) and extragalactic (shaded region [151]). Gray symbols are experimental upper limits (diamonds — GRAPES-3 [152, 153], empty triangles — KASCADE [154], upward triangles — KASCADE and KASCADE-Grande [155], downward triangles — EAS-MSU [156], horizontal dashes — CASA-MIA [157], asterisks — EAS-TOP [158], squares — preliminary analysis of Tibet-ASγ in Ref. [159]).

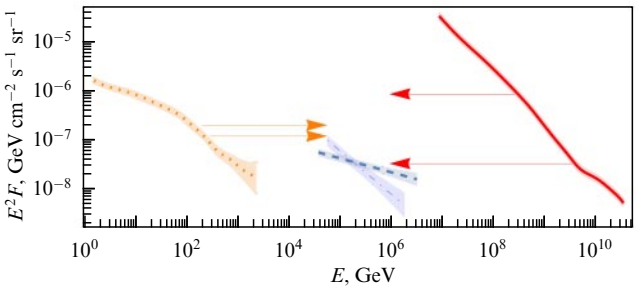

Figure 22. Constraints on and estimates of neutrino flux in the multimessenger approach. On the left, $E \sim 1-1000$ GeV (orange dashed line — diffuse isotropic gamma ray flux according to Fermi LAT data [168]). In the middle, $E \sim 10^5-10^6$ GeV — total fluxes of astrophysical neutrinos of all flavors according to IceCube data (blue dashed line — ν_μ 2019 [25]; thin blue dashed-dotted line — HESE 2020 [24]). On the right, $E \sim 10^7-10^{10}$ GeV — cosmic-ray flux according to the combined fit [169]. Arrows illustrate the estimates and constraints discussed in the text and their uncertainties.

the Fermi satellite, so that the flux obtained by cascading companion photons from neutrino sources in no way can exceed these measurements. Such a requirement allows an upper limit to be set on the diffuse neutrino flux from extragalactic sources [143], unless they themselves absorb all photons with energies $\gtrsim 10$ GeV. The quantitative value of this limit depends, although not too much, on assumptions about the shape of the neutrino spectrum, on the mechanism (pp or pγ), and, most importantly, on the distribution of sources in the Universe (evolution). On the other hand, the contribution of galactic sources can be estimated from observations of photons with $E_\gamma \sim 2E_\nu$, which within the Galaxy can reach the observer almost without absorption (Fig. 21). In the context of IceCube measurements, these possibilities have been investigated, for example, in papers [151, 160–165].

A similar construction, albeit one requiring many more assumptions, can also be built for cosmic rays. This widely known estimate has been called the Waxman–Bahcall limit [145], although, as we shall see below, it gives some characteristic value of the flux rather than constraining it from above. Let us suppose that all cosmic rays of ultra-high energy detected by appropriate detectors are accelerated in some extragalactic sources, and determine the number of high-energy protons from measured fluxes at energies of $\sim 10^{19}$ eV (at these energies cosmic rays are guaranteed to be extragalactic in origin). The same mechanism that accelerates some protons to the highest energies would accelerate many more protons to lower energies, $\sim 10^{16}-10^{17}$ eV. In contrast to the most energetic ones, the protons at lower energies are trapped by the magnetic field in the source, and sooner or later interact there with matter or radiation, giving rise to π mesons. The neutrino flux that would be produced if the energy of all these protons were transferred to the π mesons, decaying into photons and neutrinos [145], gives by construction an upper limit on neutrino fluxes (this energy may remain in cosmic rays or be re-emitted in other ways). However, soon after the publication of this estimate, it became clear that it contains too many assumptions [166], first of all, the rather finely tuned assumption that cosmic rays with energies of $\sim 10^{19}$ eV leave the source, but protons of lower energy, those producing the observed neutrinos, stay there. It is unclear whether cosmic rays of ultra-high energies and neutrinos of energies of ~ 100 TeV must be produced in the same sources, since to accelerate protons to $\sim 10^{19}$ eV it would require much more exotic and difficult to achieve conditions than those necessary for the neutrino-producing protons of $E_p \sim 20E_\nu \sim 10^{16}$ eV. Finally, there is still no clarity as to which energies cosmic rays detected on Earth have an extragalactic origin, while the numerical value of the obtained estimate depends considerably on this.

The appealing simplicity of these estimates has been one of the important motivations for building cubic-kilometer scale neutrino telescopes, whose sensitivity just reaches such flux values [167]. Surprisingly, the observed IceCube neutrino fluxes are, by order of magnitude, close to these estimates, understood as upper limits, although originally this could not have been predicted:

''Experiments with extragalactic neutrinos..., given a positive result, will provide very important and unique information both for astrophysics and for elementary-particle physics. If the result is negative (with an installation of 10^9 m^3), this will merely give cause to the mournful arguments by the astrophysicists, who will undoubtedly find many 'natural' explanations for the low flux of extragalactic neutrinos'' (V S Berezinskii, G T Zatsepin [167]).

One might even say that one of the major difficulties in the theoretical explanation of the origin of detected astrophysical neutrinos is precisely that their flux turns out to be very large, at the level of maximal expectations. And these estimates have also remained in the focus of more detailed studies of the neutrino origin.

Let us take a look at Fig. 22. Similar plots are often used to illustrate the multimessenger approach. It shows the energy fluxes of diffuse photons, neutrinos, and cosmic rays recorded by different instruments at the corresponding energy ranges. One can note that the fluxes of neutrinos of $\sim$ PeV, photons of ~ 10 GeV, and protons of $\sim 10^{19}$ eV are of the same order of magnitude, $\sim 10^{-8}$ GeV cm^{-2} s^{-1} sr^{-1}. This allows us to speculate about the realization of the scenario described above, saturating the multimessenger constraints (neutrinos are born in extragalactic sources of ultra-high energy cosmic rays, and diffuse gamma rays are the result of electromagnetic

cascades triggered by photons born jointly with the neutrinos). For neutrinos with energies above 100 TeV, such models can indeed be proposed [170]. However, on closer examination, for the neutrino flux of all energies, such reasoning looks superficial and probably incorrect:

(1) the neutrino fluxes registered by IceCube in the cascade mode, at energies up to ~ 50 TeV, violate the Fermi-LAT upper limit and exceed the Waxman–Bahcall estimate;

(2) a significant fraction of the diffuse photon flux recorded by Fermi LAT is associated with numerous distant blazars, which are not resolvable into individual point sources due to imperfections in the instrument [171], and these blazars may be neutrino sources themselves;

(3) the cosmic-ray spectrum decreases rapidly, and the assertions of approximate equality of energy fluxes are only valid for certain energies; it is unclear how these energies are singled out compared to somewhat smaller ones, $\sim 3\times 10^{17}$ eV, at which cosmic rays are also likely extragalactic (for quantitative estimates, see Ref. [172]).

As discussed above, other observational evidence also suggests that the picture of the neutrino origin is more complex.

Other regimes and mechanisms. Let us briefly mention possible variations in the standard picture based on π-meson decays, discussed above, while remaining within the Standard Model of particle physics.

Muon-damp regime. If the decays of $\pi^{\pm}$-mesons occur in the region of a strong magnetic field, the relatively long-lived $\mu^{\pm}$ have time to lose a significant fraction of their energy to synchrotron radiation before decaying. In this case, all of the high-energy neutrinos are muon neutrinos directly born from $\pi^{\pm}$, that is, in formulas (12) we should put $f_e^0 = 0$. Oscillations result in a flavor composition different from the standard one: the average flux of ν_e and ν_τ is no longer equal to that of ν_μ, but to $\sim 2/3$ of it. The current accuracy of the determination of composition is still insufficient to reliably distinguish between these scenarios (see Fig. 12). This scenario, and even more exotic ones, are discussed, for example, in Refs [173, 174]. The magnetic field at which this mode starts to work can be estimated from the requirement that the characteristic synchrotron-loss time of the muon be less than its lifetime, while the muon energy can be related to that of the neutrino. It turns out that, to damp the muons, the field must exceed

$$B_{\mu\,\mathrm{damp}} \approx 60\ \mathrm{kG}\left(\frac{E_\nu}{100\ \mathrm{TeV}}\right)^{-1}.$$

Fields of the order of 10^4 G may be present in the immediate neighborhoods of supermassive black holes, so further refinement of the flavor composition of observed neutrinos could isolate or constrain this class of potential sources [175]. Note that the number of photons from π^0 decays per high-energy neutrino in this case is larger than for the usual scenario.

Note about beta decays. The presence of a significant number of nuclei heavier than protons among cosmic-ray particles in principle allows the following scenario for the origin of neutrinos. A nucleus, like protons, is accelerated to significant energy and then decays, for example, by photodisintegration. Some of its fragments, primarily individual neutrons, may be unstable with respect to beta decay. Neutrinos will be present among the products of the decay and inherit part of the kinetic energy of the original nucleus. This part, however, is small, since the fraction of the neutrino energy relative to the energy of the neutron is, in the laboratory frame, only $\sim 10^{-3}$. Therefore, as a rule, the contribution of such a mechanism to the production of high-energy neutrinos is small compared to that of conventional hadronic interactions. The threshold for photodisintegration of nuclei is about an order of magnitude below that for π-meson production, so there is a small energy range in which this process is significant [176]. Muon neutrinos are not produced in this case, $f_e^0 = 1$, and the observed composition, according to Eqn (12), is also depleted in ν_μ, which is in poor agreement with the IceCube results, even taking into account their low precision [24, 39].

3.2 General constraints on source populations

Each particular model of the neutrino origin makes its own predictions on the distribution of arrival directions in the sky and can be tested either in a combination of specific individual analyses or on the basis of the results outlined in Section 2.3. However, approaches exist in which, starting from observational data, it is possible to obtain general constraints on the number and the neutrino luminosity of the sources from the main population contributing to the neutrino flux. In the simplest form, mostly used today, the sources within the population are assumed to be similar; one must, however, keep in mind that realistic assumptions about natural diversity, e.g., of the luminosities of sources within the same class, may significantly alter the results of such an analysis (for a similar problem for cosmic rays of ultrahigh energies, see Refs [177–179]).

Estimate of the number of sources and their neutrino luminosity. It has already been noted above that the absence of statistically significant individual sources in the neutrino sky indicates that the observed flux either has a diffuse origin or is produced by a large number of astrophysical objects, each contributing a little to the observed neutrino flux. Here, we give quantitative estimates of these parameters.

Assume that the observed flux is produced by sources with the same neutrino luminosity and some redshift distribution (so-called cosmological evolution of sources). One can then estimate how often, for a given experimental exposure, the observation of more than one (two, three, ...) neutrino from the source ('multiplets') is expected. Comparing the number of multiplets in the data with that expected for a random distribution allows constraining the density of the number of sources in the universe for a fixed evolution. In a situation where the constraint is due to the lack of observation of significant clusters of events corresponding to point sources, it is easy to show that the assumption of the same luminosity leads to the most conservative constraint.

The method of constraining the number of sources based on the statistics of arrival-direction clustering has been proposed in Ref. [180] for ultra-high energy cosmic rays, but its application to neutrino astronomy is considerably different (see, e.g., Ref. [181]). The main difference is that cosmic rays, because of interactions with the background radiation, are collected from a limited volume of the Universe, and the absence of clusters means a large number of sources in *that volume*, that is, a *large* local source density. The neutrinos are collected from all over the Universe, and the contribution of distant (in any case numerous) sources dominates. The lack of

clusters for neutrinos indicates that there are no nearby sources standing out against the uniform background of distant and weak ones, i.e., a large distance to the nearest source or a *small* local density.[3] Of course, in the analysis, one has to account for the large number of random clusters from atmospheric neutrinos. On the other hand, unlike charged cosmic rays, neutrinos propagate in straight lines, so the angular size of the cluster is completely determined by the precision of the arrival direction.

Knowing the average neutrino luminosity of each source and the distribution of sources by distance, i.e., the input data for estimating the statistics of event clusters, it is easy to calculate the total neutrino flux and to compare it with observations. The combination of the two requirements — the absence of significant point sources or clusters of events and an explanation of the observed flux — allows one to constrain the combinations of neutrino luminosity and source number density for a fixed assumption about their cosmological evolution. Variations of this approach have been applied to constraining the parameters of neutrino sources in Refs [183–189].

In Fig. 23, results are presented for models with fast positive evolution (many sources at large redshifts), characteristic for active galactic nuclei. The constraints on high ($E_\nu > 200$ TeV) and all (i.e., mostly $\gtrsim 10$ TeV) energies, obtained from track events, are shown separately. The combination of the required neutrino luminosity and the statistics of arrival-direction clusters places serious constraints on the models of sources. In particular, the neutrino luminosity of a typical source appears to be substantially smaller than the characteristic photon luminosity of objects of this type. The most severe constraints for specific classes of sources arise if, in addition to clustering, i.e., autocorrelation of neutrino arrival directions, one takes into account the cross correlation of neutrinos and directions to the sources (see Section 2.3.3) [188]. For instance, in Fig. 23, the region of the characteristic parameters of VLBI-selected blazars, Section 2.3.3 [67, 85], is shown. To explain the observed flux, their neutrino luminosity must be of the order of a few percent of the luminosity in photons. It can be seen that, in this case, they can be sources of all astrophysical neutrinos, both of those with energies above 200 TeV and of those with lower energies, in agreement with the observed directional correlations.

As for sources with weak evolution, constraints similar to those shown in Fig. 23 are satisfied only for low neutrino luminosity and high source number densities. For densities of $\gtrsim 10^{-6}$ Mpc^{-3}, these constraints require taking into account [190] the local large-scale structure of the Universe, which the distributions of all astrophysical objects follow, when analyzing neutrino arrival directions; examples of sources of this type are starburst galaxies. The analyses carried out in [191, 192] have not yielded strong constraints on these scenarios yet.

3.3 Conclusions about general constraints

A multimessenger analysis of diffuse fluxes of extragalactic cosmic rays, GeV gamma rays, and high-energy astrophysical neutrinos demonstrates that the neutrino fluxes detected by IceCube are at the level of upper limits, i.e., the highest

[3] A lack of clusters both in cosmic rays and in neutrinos therefore suggests that it would be unlikely to observe cross correlations between their arrival directions [182].

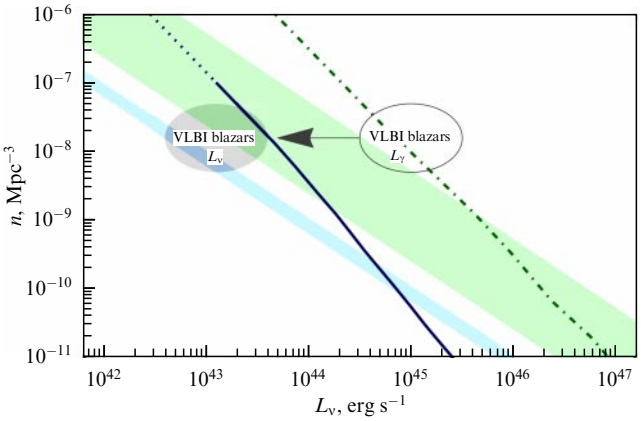

Figure 23. Constraints on the source number density n (at redshift $z = 0$) and their typical neutrino luminosity L_ν. Dashed line — upper limit (99% CL) on n from the absence of significant neutrino point sources in the track sample of 8 years of IceCube data [189]; wide shaded band — allowed (99% CL) region in which these sources explain the flux and spectrum of IceCube from the same data [189]. Solid line (dotted line is its extrapolation) is the upper limit (95% CL) on n from the absence of clusters of neutrino arrival directions in a sample of IceCube tracks with energies > 200 TeV [187]; narrow shaded band is the allowed (68% CL) region in which these sources explain the flux and spectrum from the same IceCube data [187]. Constraints assume a strong positive evolution typical of active galactic nuclei. Shaded ellipse is an estimate of the characteristic parameters of VLBI-selected blazars (see Section 2.3.3). Empty ellipse is the same but assuming equality of neutrino and bolometric gamma-ray luminosities.

theoretical expectations, for extragalactic sources with the π-meson mechanism. Of course, particular quantitative limits depend on the details of the model, but qualitatively the picture indicates that the observed particle fluxes in the three channels — cosmic rays, neutrinos, and photons — are consistent with each other in order of magnitude. This allows the possibility that proton interactions play a significant role in the origin not only of neutrinos but also of high-energy gamma rays. Note that, prior to the IceCube observations, the origin of the bulk of astrophysical high-energy gamma rays was usually attributed to relativistic electrons.

At the same time, results of studies of neutrino arrival directions, primarily their diffuse nature — the lack of clearly identified sources making a significant contribution to the flux; the lack of neutrino correlations with populations of gamma-ray bright potential sources; strong constraints on the Galactic-disk excess in the neutrino flux — point to difficulties with the naive multimessenger approach. It is not possible to satisfy all constraints simultaneously or to explain all observations in a simple model with a single class of sources. It is possible that the observed flux of high-energy astrophysical neutrinos comes from different classes of sources, which include both galactic 'PeVatrons,' which dominate at lower energies, and extragalactic ones (e.g., radio blazars), which provide a harder spectrum. At the same time, the number of extragalactic sources contributing to the observed flux is large, and the neutrino luminosity of each of them is orders of magnitude smaller than the photon luminosity.

4. Potential source classes

Staying within the frameworks of the general picture derived from observational constraints and described at the end of the

previous section, we will very briefly list here specific astrophysical objects and environments which are potential sources of observed neutrinos.

4.1 Models of extragalactic sources

Active galactic nuclei. Environments of supermassive black holes in active galactic nuclei are the most powerful steady sources of radiation in the Universe. Relativistic blazar jets directed towards the observer result in a strong enhancement of fluxes of both photons and neutrinos due to the Lorentzian kinematics. They have been considered as sources of high-energy neutrinos in theoretical studies since the early days of neutrino astronomy [193–195] (see also recent reviews [196–199] and references therein).

The classical scenario [200–207] involves neutrino production in the vicinity of a black hole, closer than jet launches. The density of matter in the central regions of galactic nuclei is low, and the main channel for the neutrino production is probably the $p\gamma$ process. Relativistic protons with the required energies up to $\sim 10^{16}-10^{17}$ eV can be accelerated either in the black-hole magnetosphere [208] or in shock waves in the vicinity of the accretion disk. The latter is also the source of intense radiation that provides the second necessary ingredient, target photons.

In the context of the observational data discussed above, this scenario requires extension or modification, because it does not allow an explanation of astrophysical neutrinos of energies on the order of 10 TeV, for which a connection to blazars has also been established [85]. Indeed, according to Eqn (9), production of these neutrinos requires X-ray target photons, while the accretion disk emits mainly in the ultraviolet band and can provide target photons for the production of neutrinos of much higher energies only. Modifications of this scenario include a contribution from the emission of the accretion disk corona [209–212] whose spectrum, compared to the disk itself, extends into higher energies, although with a lower intensity. A common problem of models of neutrino production in the region of the disk and its corona is the lack of a direct link to relativistic amplification in jets — as a rule, neutrinos in such models are emitted isotropically. An additional, albeit avoidable, complication is related to the fact that, judging by the fast variability, the observed gamma rays from the blazars originate precisely in this region, while no statistically significant association between neutrinos and such gamma rays were found.

These problems are circumvented if neutrinos are born already in relativistic jets, near their base (see, e.g., [85, 213, 214]). Here, X-ray photons of the target are present, and the acceleration of protons to the desired energies can occur in weakly relativistic shock waves [215–217]. This is where the visible radio emission of blazars is produced, correlations of neutrino arrival moments with enhancements which have been established in [67, 90] (regions closer to the black hole are opaque to radio emission). Since one-zone models fail to describe the entire spectrum of the observed electromagnetic radiation of blazars from radio to gamma rays, it is natural to assume that the neutrino radiation may not come from the same region as the gamma radiation. However, it is worth noting that the target photon density in the jet is small, and to produce the required number of neutrinos in this region one needs a significant proton power of the jet [85]. It could be possible that the observed correlation between neutrinos and the radio emission indicates the operation of the pp-mechanism [218].

Cosmic-ray reservoirs. This class includes astrophysical objects of various scales where cosmic rays are trapped for long periods by a magnetic field. The probability of their interaction with ambient protons grows with time, so that eventual neutrino production by the pp-mechanism is guaranteed. One of the most widely discussed source classes of this kind is starburst galaxies, which have magnetic fields large enough to confine protons and where mechanisms to accelerate cosmic protons to high energies may work. Reference [219], prior to the start of IceCube data taking, predicted diffuse neutrino flux from a population of starburst galaxies at the level of the subsequently discovered flux. Sources of this class are prototypical for the Waxman–Bahcall estimate, and all the multimessenger relations and constraints discussed in Section 3.1 work for them. In particular, such sources are transparent to gamma rays, but are not blazars, so the 'cascade' limit from the Fermi LAT is particularly serious [220, 221]. Reservoirs of cosmic rays, which in addition to starburst galaxies also include clusters of galaxies [222, 223] and kiloparsec-scale structures in active galaxies, radio lobes [224], can therefore be sources of observable neutrinos only with energies $\gtrsim 100$ TeV [225]. Interest in this class of sources is spurred [226] by an excess of IceCube events from the direction of the nearby powerful starburst galaxy NGC 1068 (see Section 2.3.2), but no analysis of the source population confirms a significant contribution from cosmic-ray reservoirs to the neutrino flux.

Stopped jets. In explosions of very massive stars, not uncommon, in particular at the early stages of galaxy evolution, is the fact that the jets produced in the central part of the star may not reach the surface because of the high density of the hydrogen envelope of the star. The result is a 'choked gamma-ray burst,' an event with the energy release of a cosmic gamma-ray burst but without a detectable flare of electromagnetic radiation, which is absorbed by the outer layers of the star and/or the surrounding matter. In the process of interaction of the jets with matter, neutrinos are born in pp-interactions [227–231], and, because of the lack of visible gamma-ray bursts, there is no contradiction with the constraints from a population analysis [232, 233]. Theoretical models of such sources contain considerable uncertainties, but a common feature is a strong peak in the energy distribution of neutrinos near 100 TeV. As a consequence, such sources cannot explain the entire observed neutrino flux: either the observed flux at ~ 100 TeV is explained but not the flux below or above that, or the predicted flux at 100 TeV is too high [234–239].

Tidal disruption of stars. A star falling into a supermassive black hole is a rare event. On average, in a particular galaxy, it happens once every 10^4-10^5 years. The star is first destroyed by tidal forces and then about half of its matter accretes onto the black hole. A sharp increase in the accretion rate leads in any case to a flare and, rarely, to the formation of a jet. One can understand this event as a short-term transformation of an ordinary galaxy into an active one, so that neutrinos can be produced in the jet in the usual $p\gamma$ process. Moreover, the remnants of the star provide additional target material for the pp process. The majority of theoretical studies on the neutrino production in tidal disruption events address processes with the formation of jets [240–247], to which the case of a registered coincidence with the IceCube event [125] does not seem to belong [126, 248]. The contribution of tidal

disruption events without jet formation to the observed high-energy neutrino flux can only be very small, as follows both from a theoretical point of view [248] and from population analysis [124].

4.2 Models of the Galactic flux component

When discussing possible scenarios for the origin of neutrinos in our Galaxy, one should not forget about strict observational constraints on neutrinos from the Galactic disk (see Section 2.3.1, Fig. 15). The constraints on the disk contribution (and the first indications of its observations) are on the order of 10% of the total neutrino flux, in agreement with expectations for the guaranteed flux from cosmic-ray interactions with the interstellar gas. Successful scenarios for the origin of the dominant part of the neutrino flux in the Galaxy must somehow circumvent these disk-related constraints. There are two possibilities:

(1) the flux comes from sources not related to the disk, i.e. distributed in the Galactic halo (circumgalactic gas or halo dark matter);

(2) the main contribution to the flux comes from the immediate neighborhood of the Solar System, that is, from a region smaller in size than the thickness of the disk.

In addition, the sources can be individual rare objects or regions in the Galactic plane whose distribution does not follow the distribution of the disk's gamma rays, which is assumed in the derivation of constraints of Section 2.3.1.

Circumgalactic gas. In recent years, a variety of observational evidence has been obtained ([249]; see, e.g., [250] and references therein) of the existence of an extended halo of circumgalactic gas around our Galaxy, extending up to its virial radius, i.e., about 200 kpc (recall that the radius of the Galactic disk is about 20 kpc, and its thickness is < 1 kpc). At energies of $\gtrsim 10^{17}$ eV, cosmic protons leave the Galactic disk and, interacting with the gas, can produce high-energy photons [251] and neutrinos [252]. Under the assumption of symmetric diffusion of cosmic rays and for a realistic model of the circumgalactic gas, the neutrino flux from such interactions is only a few percent of the observed one [253], but it may be possible that either feeding the halo with cosmic rays through Fermi bubbles or other manifestations of past activity in our Galactic nucleus could alter this result [254].

Decays of dark-matter particles. Convincingly confirmed by astronomical observations at various scales, the existence of invisible matter in the Universe has yet to be firmly explained in terms of particle physics. There are many working models, attracting more and more attention, while the scenario of weakly interacting massive particles, most popular for decades, is gradually being ruled out experimentally (see, e.g., the discussion in Ref. [255]). Astrophysical neutrinos can be produced in the decays of dark-matter particles [256–259]; to produce decay products of the energies discussed, the dark-matter particles must be superheavy [260, 261]. In the context of explaining the IceCube results, this scenario has been discussed in particular in Refs [262–267]. The entire observed neutrino spectrum from tens of TeV to tens of PeV cannot be explained in this way, because the energy distribution of the decay products is noticeably narrower, but this mechanism can explain the observed flux at some energies. Even for purely lepton decay channels, very strict constraints on such a scenario are given by the lack of observation of an accompanying flux of high-energy photons [268–271].

Gas bubbles and star formation regions. In the Galactic disk, neutrinos can be produced in interactions of cosmic rays with protons and nuclei of the interstellar gas, but both are unevenly distributed across the disk. Cosmic rays are accelerated in sources, 'PeVatrons,' and are trapped in regions of strong magnetic fields, while the distribution of gas is complex because of stellar winds and shock waves from supernova explosions. As a consequence, the neutrino signal from the disk may be dominated by the contribution of a few regions of intense star formation [272–275], which look like compact clusters of young massive stars, and so-called superbubbles. A special place is the Local Bubble, within which our Solar System resides: the neutrinos coming from it [149, 150, 276] do not point back to the Galactic disk, since the size of the bubble, ~ 100 pc, is noticeably smaller than the thickness of the disk. Sources of this type include the Cygnus Cocoon, mentioned in Section 2.3.4 in connection with registration from of a flare of photons with energies above 300 TeV, coinciding with an IceCube neutrino event [134]. Note that the available constraints will also be satisfied by neutrinos from other rare objects, whose distribution in the sky does not follow the profile of the Galactic gas, such as microquasars in gamma-ray bright binary systems, one of which coincides, within the accuracy of determining the arrival direction of neutrinos and photons discussed above, with the Cygnus Cocoon [277].

Contribution of similar galaxies. Speaking of the Galactic origin of neutrinos, we should not forget that our Galaxy is not unique and sources like these are present not only in it, but also in billions of other galaxies. Although the contribution of the sources in our immediate vicinity is significant, neutrinos are collected from all over the Universe, and the total contribution from other galaxies may be of the same order as ours. Simple quantitative estimates [278] show that this is indeed the case: by order of magnitude, any Galactic contribution to the persistent flux of high-energy neutrinos would be similar to the total contribution of similar sources in all other galaxies in the Universe.

5. Conclusions

• Astrophysical neutrinos of high energies (10 TeV–10 PeV) have been reliably detected by the IceCube experiment; their observation is being confirmed by the ANTARES results and by the first Baikal-GVD data. The distribution in zenith angles of events passing the strictest selection excludes their atmospheric origin even for exotic assumptions. In the energy range above 100 TeV, neutrino astronomy has surpassed photon astronomy and motivated its development.

• Although the sources of high-energy astrophysical neutrinos have not yet been definitively determined, their total fluxes point to a significant role of relativistic hadrons in high-energy astrophysics: within standard physics, only processes involving them can give rise to neutrinos of this energy range.

• Spectra of astrophysical neutrinos reconstructed from IceCube cascade and track events are not very consistent with each other under the assumption of a power-law dependence of the flux on the energy. This can be explained by the more complex shape of the spectrum, reflecting the combined contribution of different populations of sources. It is likely that the sky in neutrinos looks no less complex and diverse as in photons.

• The flux of astrophysical neutrinos at energies above ~ 100 TeV is probably dominated by the contribution of numerous distant extragalactic sources. Population studies indicate a statistically significant association of neutrinos with blazars, that is, active galactic nuclei with relativistic jets directed toward the observer, manifesting themselves by powerful radiation from parsec scales visible with VLBI. These sources are not always bright in the gamma-ray band, and their neutrino luminosity on average is noticeably lower than the photon luminosity. They contribute significantly to the neutrino flux also at lower energies.

• The neutrino flux component that dominates at energies of $\sim 10-100$ TeV may either be of a Galactic origin or be connected to multiple extragalactic sources which are opaque to photons at $\gtrsim$ GeV energies. There are observational indications of the presence of a Galactic component.

• The prospects for further understanding the nature of high-energy astrophysical neutrinos are related both to the work of cubic-kilometer scale neutrino telescopes (including Northern hemisphere water detectors, Baikal-GVD, which has just started work, and KM3NeT, which is under construction) and to multimessenger analysis, including observations in the electromagnetic channel in all bands — from radio (in which, due to the best angular resolution, it is possible to study blazar jets in the immediate vicinity of supermassive black holes) to PeV (this emerging field of astronomy will answer questions about Galactic sources of neutrinos).

Acknowledgments

The author is indebted for interesting and helpful discussions of various aspects related to the origin of high-energy astrophysical neutrinos to his colleagues, M Barkov, A Bykov, H Dembinski, T Dzhaddoev, Zh-A Dzhilkibaev, G Domogatsky, K Zhuravleva, O Kalashev, Yu A and Yu Yu Kovalev, M Kuznetsov, T Montaruli, K Murase, A Neronov, A Plavin, E Podlesny, K Postnov, V Rubakov, G Rubtsov, K Ryabtsev, D Samtleben, D Semikoz, O Suvorova, A Franckowiak, and C Spiering.

This study was supported by the Ministry of Science and Higher Education of the Russian Federation, Contract 075-15-2020-778 of the Program of Major Scientific Projects within the National Project Science.

References

1. Capone A, Lipari P, Vissani F, in *Multiple Messengers and Challenges in Astroparticle Physics* (Eds R Aloisio, E Coccia, F Vissani) (Cham: Springer Intern. Publ., 2018) p. 195
2. Spurio M *Probes of Multimessenger Astrophysics*: *Charged Cosmic Rays, Neutrinos, γ-Rays and Gravitational Waves* (New York: Springer, 2018)
3. Palladino A, Spurio M, Vissani F *Universe* **6** 30 (2020)
4. Spiering Ch *Phys. Usp.* **57** 470 (2014); *Usp. Fiz. Nauk* **184** 510 (2014)
5. Spiering C "Neutrino detectors under water and ice", in *Particle Physics Reference Library* (Eds C Fabjan, H Schopper) (Cham: Springer, 2020)
6. Ryabov V A *Phys. Usp.* **49** 905 (2006); *Usp. Fiz. Nauk* **176** 931 (2006)
7. Glashow S L *Phys. Rev.* **118** 316 (1960)
8. Berezinskii V S, Gazizov A Z *JETP Lett.* **25** 254 (1977); *Pis'ma Zh. Eksp. Teor. Fiz.* **25** 276 (1977)
9. Aartsen M G et al. *Astrophys. J.* **835** 151 (2017)
10. Learned J G, Pakvasa S *Astropart. Phys.* **3** 267 (1995)
11. Aartsen M G et al. (IceCube Collab.) *Phys. Rev. D* **93** 022001 (2016)
12. Aartsen M G et al. *Nature* **591** 220 (2021)
13. Abbasi R et al., arXiv:2011.03561
14. Troitsky S V, in *Mnogokanal'naya Astronomiya* (Multimessenger Astronomy) (Ed. A M Cherepashchuk) (Fryazino: Vek-2, 2019) p. 135
15. Aartsen M G et al. *Science* **361** eaat1378 (2018)
16. Chiarusi T, Spurio M *Eur. Phys. J. C* **65** 649 (2010)
17. Aartsen M G et al. *Astrophys. J.* **833** 3 (2016)
18. IceCube catalog of alert events up through IceCube-170922A (Posted on July 12, 2018), https://doi.org/10.21234/B4KS6S
19. All-sky point-source IceCube data: years 2008-2018 (Posted on January 26, 2021), https://doi.org/10.21234/sxvs-mt83
20. Abbasi R et al. (IceCube Collab.), arXiv:2101.09836, https://doi.org/10.21234/CPKQ-K003
21. Aartsen M G et al. (IceCube Collab.) *Phys. Rev. Lett.* **113** 101101 (2014)
22. Aartsen M G et al. (IceCube Collab.), in *34th Intern. Cosmic Ray Conf., ICRC 2015, 30 July–6 August 2015, The Hague, Netherlands*
23. Aartsen M G et al. (IceCube Collab.), arXiv:1710.01179
24. Abbasi R et al. (IceCube Collab.) *Phys. Rev. D* **104** 022002 (2021)
25. Stettner J (IceCube Collab.) *PoS* **ICRC2019** 1017 (2020)
26. Markov M A, in *Proc. of the 10th Intern. Conf. on High-Energy Physics, ICHEP 60, Rochester, NY, USA, 25 August – 1 September 1960* (Eds E C G Sudarshan, J H Tinlot, A C Melissinos) (Rochester, NY: Rochester Univ., 1960) p. 578
27. Zheleznykh I *Int. J. Mod. Phys. A* **21** (Suppl. 01) 1 (2006)
28. Fusco L A, Versari F *PoS* **ICRC2019** 891 (2020)
29. Avrorin A D et al. *PoS* **ICRC2019** 873 (2021)
30. Aartsen M G et al. (IceCube Collab.) *Phys. Rev. Lett.* **125** 121104 (2020)
31. Aartsen M G et al. (IceCube Collab.) *Phys. Rev. D* **91** 022001 (2015)
32. Aartsen M G et al. (IceCube Collab.) *Phys. Rev. D* **99** 032004 (2019)
33. Fargion D, Oliva P, Ucci G *PoS* **FRAPWS2014** 028 (2016)
34. Mascaretti C, Vissani F *JCAP* **2019** (08) 004 (2019)
35. Fargion D et al. *PoS* **FRAPWS2018** 007 (2019)
36. Palladino A, Mascaretti C, Vissani F *JCAP* **2018** (08) 004 (2018)
37. Chen C-Y, Bhupal Dev P S, Soni A *Phys. Rev. D* **92** 073001 (2015)
38. Halzen F *PoS* **ICRC2019** 021 (2020)
39. Bustamante M, Ahlers M *Phys. Rev. Lett.* **122** 241101 (2019)
40. Song N et al. *JCAP* **2021** (04) 054 (2021)
41. Vincent A C, Palomares-Ruiz S, Mena O *Phys. Rev. D* **94** 023009 (2016)
42. Palladino A, Vissani F *Astrophys. J.* **826** 185 (2016)
43. Neronov A, Semikoz D *Phys. Rev. D* **93** 123002 (2016)
44. Palladino A, Spurio M, Vissani F *JCAP* **2016** (12) 045 (2016)
45. Troitsky S V *Phys. Usp.* **56** 304 (2013); *Usp. Fiz. Nauk* **183** 323 (2013)
46. Aartsen M G et al. *Astrophys. J.* **835** 151 (2017)
47. All-sky point-source IceCube data: years 2012-2015 (Posted on February 27, 2020), https://doi.org/10.21234/exm3-tm26
48. Aartsen M G et al. (IceCube Collab.), arXiv:1710.01179
49. Ando S, Tamborra I, Zandanel F *Phys. Rev. Lett.* **115** 221101 (2015)
50. Gaggero D et al. *Astrophys. J. Lett.* **815** L25 (2015)
51. Albert A et al. *Astrophys. J. Lett.* **868** L20 (2018)
52. Aartsen M G et al. *Astrophys. J.* **886** 12 (2019)
53. Neronov A, Semikoz D *Astropart. Phys.* **75** 60 (2016)
54. Troitsky S *JETP Lett.* **102** 785 (2015); *Pis'ma Zh. Eksp. Teor. Fiz.* **102** 899 (2015)
55. Dubovsky S L, Tinyakov P G *JETP Lett.* **68** 107 (1998); *Pis'ma Zh. Eksp. Teor. Fiz.* **68** 99 (1998)
56. Argüelles C A, Dujmovic H *PoS* **ICRC2019** 839 (2020)
57. Dekker A, Chianese M, Ando S *JCAP* **2020** (09) 007 (2020)
58. Aartsen M G et al. (IceCube Collab.) *Eur. Phys. J. C* **78** 831 (2018)
59. Bhattacharya A et al. *JCAP* **2019** (05) 051 (2019)
60. Su M, Slatyer T R, Finkbeiner D P *Astrophys. J.* **724** 1044 (2010)
61. Hallmann S, Eberl T et al. *PoS* **ICRC2017** 1001 (2018)
62. Lunardini C et al. *Phys. Rev. D* **90** 023016 (2014)
63. Fang K et al. *Phys. Rev. D* **96** 123007 (2017)
64. Tinyakov P G, Tkachev I I *Phys. Rev. D* **69** 128301 (2004)
65. Aartsen M G et al. *Phys. Rev. Lett.* **124** 051103 (2020)
66. Albert A et al. *Astrophys. J.* **892** 92 (2020)
67. Plavin A et al. *Astrophys. J.* **894** 101 (2020)
68. Giommi P et al. *Mon. Not. R. Astron. Soc.* **497** 865 (2020)
69. Aartsen M G et al. *Astrophys. J.* **898** 117 (2020)
70. Smith D, Hooper D, Vieregg A *JCAP* **2021** (03) 031 (2021)
71. Albert A et al. *Astrophys. J.* **911** 48 (2021)
72. Padovani P, Turcati A, Resconi E *Mon. Not. R. Astron. Soc.* **477** 3469 (2018)
73. Acero F et al. *Astrophys. J. Suppl.* **218** 23 (2015)

74. Ackermann M et al. *Astrophys. J. Suppl.* **222** 5 (2016)
75. Ajello M et al. *Astrophys. J. Suppl.* **232** 18 (2017)
76. Ackermann M et al. *Astrophys. J.* **810** 14 (2015)
77. Ajello M et al. *Astrophys. J.* **892** 105 (2020)
78. Chang Y-L, Brandt C H, Giommi P *Astron. Comput.* **30** 100350 (2020)
79. Chang Y L et al. *Astron. Astrophys.* **598** A17 (2017)
80. Chang Y L et al. *Astron. Astrophys.* **632** A77 (2019)
81. Neronov A, Semikoz D V, Ptitsyna K *Astron. Astrophys.* **603** A135 (2017)
82. Palladino A, Vissani F *Astron. Astrophys.* **604** A18 (2017)
83. Padovani P et al. *Mon. Not. R. Astron. Soc.* **457** 3582 (2016)
84. Huber M *PoS* **ICRC2019** 916 (2020)
85. Plavin A V et al. *Astrophys. J.* **908** 157 (2021)
86. Zhou B, Kamionkowski M, Liang Y *Phys. Rev. D* **103** 123018 (2021)
87. Zensus J A *Annu. Rev. Astron. Astrophys.* **35** 607 (1997)
88. Blandford R, Meier D, Readhead A *Annu. Rev. Astron. Astrophys.* **57** 467 (2019)
89. Thompson A R, Moran J M, Swenson G W (Jr.) *Interferometry and Synthesis in Radio Astronomy* 3rd ed. (Cham: Springer Intern. Publ., 2017)
90. Hovatta T et al. *Astron. Astrophys.* **650** A83 (2021)
91. Aublin J, Plavin A *PoS* **ICRC2021** 1164 (2021)
92. Murase K, Bartos I *Annu. Rev. Nucl. Part. Sci.* **69** 477 (2019)
93. Strotjohann N L, Kowalski M, Franckowiak A *Astron. Astrophys.* **622** L9 (2019)
94. Ackermann M "Searches for signals from cosmic point-like sources of high energy neutrinos in 5 years of AMANDA-II data", Ph.D. Thesis (Berlin: Humboldt Univ., 2006); https://edoc.hu-berlin.de/handle/18452/16219
95. Bernardini E *Nucl. Instrum. Meth. Phys. Res. A* **567** 418 (2006)
96. Halzen F, Hooper D *Astropart. Phys.* **23** 537 (2005)
97. Reimer A, Bottcher M, Postnikov S *Astrophys. J.* **630** 186 (2005)
98. Kintscher T et al. *PoS* **ICRC2017** 969 (2018)
99. Lipunov V M et al. *Astrophys. J. Lett.* **896** L19 (2020)
100. Aartsen M G et al. *Science* **361** 147 (2018)
101. Halzen F et al. *Astrophys. J. Lett.* **874** L9 (2019)
102. Gao S et al. *Nat. Astron.* **3** 88 (2019)
103. Cerruti M et al. *Mon. Not. R. Astron. Soc.* **483** L12 (2019)
104. Cerruti M et al. *Mon. Not. R. Astron. Soc.* **502** L21 (2021) Erratum
105. Keivani A et al. *Astrophys. J.* **864** 84 (2018)
106. Murase K, Oikonomou F, Petropoulou M *Astrophys. J.* **865** 124 (2018)
107. Gokus A et al. *Astron. Nachr.* **339** 331 (2018)
108. Sahakyan N *Astrophys. J.* **866** 109 (2018)
109. Reimer A, Boettcher M, Buson S *Astrophys. J.* **881** 46 (2019)
110. Reimer A, Boettcher M, Buson S *Astrophys. J.* **899** 168 (2020) Erratum
111. Rodrigues X et al. *Astrophys. J. Lett.* **874** L29 (2019)
112. Kovalev Y A et al. *Adv. Space Res.* **65** 745 (2020)
113. Postnov K A *Phys. Usp.* **42** 469 (1999); *Usp. Fiz. Nauk* **169** 545 (1999)
114. Bykov A M *Phys. Usp.* **61** 805 (2018); *Usp. Fiz. Nauk* **188** 894 (2018)
115. Aptekar R L et al. *Phys. Usp.* **62** 739 (2019); *Usp. Fiz. Nauk* **189** 785 (2019)
116. Milgrom M, Usov V *Astrophys. J. Lett.* **449** L37 (1995)
117. Waxman E *Phys. Rev. Lett.* **75** 386 (1995)
118. Vietri M *Astrophys. J.* **453** 883 (1995)
119. Waxman E, Bahcall J *Phys. Rev. Lett.* **78** 2292 (1997)
120. Aartsen M G et al. *Astrophys. J.* **824** 115 (2016)
121. Aartsen M G et al. *Astrophys. J.* **843** 112 (2017)
122. Albert A et al. *Mon. Not. R. Astron. Soc.* **500** 5614 (2020)
123. Albert A et al. *JCAP* **2021** (03) 092 (2021)
124. Stein R *PoS* **ICRC2019** 1016 (2020)
125. Stein R et al. *Nat. Astron.* **5** 510 (2021)
126. Winter W, Lunardini C *Nat. Astron.* **5** 472 (2021)
127. Amenomori M et al. (Tibet ASγ Collab.) *Phys. Rev. Lett.* **123** 051101 (2019)
128. Abeysekara A U et al. *Astrophys. J.* **881** 134 (2019)
129. Albert A et al. *Astrophys. J. Lett.* **907** L30 (2021)
130. Abeysekara A U et al. (HAWC Collab.) *Phys. Rev. Lett.* **124** 021102 (2020)
131. Albert A et al. *Astrophys. J. Lett.* **896** L29 (2020)
132. Cao Z et al. *Nature* **594** 33 (2021)
133. Amenomori M et al. (Tibet ASγ Collab.) *Phys. Rev. Lett.* **126** 141101 (2021)
134. Dzhappuev D D et al. *Astrophys. J. Lett.* **96** L22 (2021)
135. Kachelriess M, Semikoz D V *Prog. Part. Nucl. Phys.* **109** 103710 (2019)
136. Berezinsky V S, Volynsky V V, in *Intern. Cosmic Ray Conf.* Vol. 10 (Tokyo: Institute for Cosmic Ray Research, Univ. of Tokyo, 1979) p. 326
137. Kelner S R, Aharonian F A, Bugayov V V *Phys. Rev. D* **74** 034018 (2006)
138. Kelner S R, Aharonian F A, Bugayov V V *Phys. Rev. D* **79** 039901 (2009) Erratum
139. Lipari P, Lusignoli M, Meloni D *Phys. Rev. D* **75** 123005 (2007)
140. Roulet E, Vissani F *JCAP* **2021** (03) 050 (2021)
141. Kudenko Yu G *Phys. Usp.* **61** 739 (2018); *Usp. Fiz. Nauk* **188** 821 (2018)
142. Zyla P A et al. *Prog. Theor. Exp. Phys.* **2020** 083C01 (2020)
143. Berezinsky V S, Smirnov A Y *Astrophys. Space Sci.* **32** 461 (1975)
144. Berezinskii V S et al. *Astrophysics of Cosmic Rays* (Ed. V L Ginzburg) (Amsterdam: North-Holland, 1990); Translated from Russian: *Astrofizika Kosmicheskikh Luchei* (Ed. V L Ginzburg) (Moscow: Nauka, 1984)
145. Waxman E, Bahcall J *Phys. Rev. D* **59** 023002 (1998)
146. Nikishov A I *Sov. Phys. JETP* **14** 393 (1962); *Zh. Eksp. Teor. Fiz.* **41** 549 (1962)
147. Berezinsky V, Kalashev O *Phys. Rev. D* **94** 023007 (2016)
148. Ackermann M et al. *Astrophys. J.* **799** 86 (2015)
149. Bouyahiaoui M, Kachelrieß M, Semikoz D V *Phys. Rev. D* **101** 123023 (2020)
150. Neronov A, Kachelrieß M, Semikoz D V *Phys. Rev. D* **98** 023004 (2018)
151. Kalashev O, Troitsky S *JETP Lett.* **100** 761 (2015); *Pis'ma Zh. Eksp. Teor. Fiz.* **100** 865 (2015)
152. Minamino M et al., in *31th Intern. Cosmic Ray Conf.* Vol. 2 (Lodz: Local Organizing Committee of ICRC, 2009) p. 1723
153. Tanaka H et al. *J. Phys. G* **39** 025201 (2012)
154. Schatz G et al., in *28th Intern. Cosmic Ray Conf.* (Tsukuba: Universal Academy Press, 2003) p. 2293
155. Apel W D et al. *Astrophys. J.* **848** 1 (2017)
156. Fomin Yu A et al. *Phys. Rev. D* **95** 123011 (2017)
157. Chantell M C et al. *Phys. Rev. Lett.* **79** 1805 (1997)
158. Aglietta M et al. *Astropart. Phys.* **6** 71 (1996)
159. Neronov A, Semikoz D, Vovk I *Astron. Astrophys.* **653** L4 (2021)
160. Murase K, Ahlers M, Lacki B C *Phys. Rev. D* **88** 121301 (2013)
161. Capanema A, Esmaili A, Murase K *Phys. Rev. D* **101** 103012 (2020)
162. Gupta N *Astropart. Phys.* **48** 75 (2013)
163. Joshi J C, Winter W, Gupta N *Mon. Not. R. Astron. Soc.* **439** 3414 (2014)
164. Joshi J C, Winter W, Gupta N *Mon. Not. R. Astron. Soc.* **446** 892 (2014) Erratum
165. Ahlers M, Murase K *Phys. Rev. D* **90** 023010 (2014)
166. Mannheim K, Protheroe R J, Rachen J P *Phys. Rev. D* **63** 023003 (2000)
167. Berezinskii V S, Zatsepin G T *Sov. Phys. Usp.* **20** 361 (1977); *Usp. Fiz. Nauk* **122** 3 (1977)
168. Neronov A, Semikoz D *Astron. Astrophys.* **633** A94 (2020)
169. Dembinski H P et al. *PoS* **ICRC2017** 533 (2018)
170. Kachelrieß M et al. *Phys. Rev. D* **96** 083006 (2017)
171. Ackermann M et al. *Phys. Rev. Lett.* **116** 151105 (2016)
172. Roulet E *JCAP* **2021** (08) 009 (2021)
173. Hummer S et al. *Astropart. Phys.* **34** 205 (2010)
174. Bustamante M, Tamborra I *Phys. Rev. D* **102** 123008 (2020)
175. Ryabtsev K, Troitsky S *Phys. Lett. B* (2021) submitted
176. Anchordoqui L A et al. *Phys. Lett. B* **593** 42 (2004)
177. Kachelriess M, Semikoz D V *Phys. Lett. B* **634** 143 (2006)
178. Ptuskin V, Rogovaya S, Zirakashvili V *Adv. Space Res.* **51** 315 (2013)
179. Kalashev O E, Ptitsyna K V, Troitsky S V *Phys. Rev. D* **86** 063005 (2012)
180. Dubovsky S L, Tinyakov P G, Tkachev I I *Phys. Rev. Lett.* **85** 1154 (2000)
181. Lipari P *Phys. Rev. D* **78** 083011 (2008)

182. Palladino A et al. *Mon. Not. R. Astron. Soc.* **494** 4255 (2020)
183. Ahlers M, Halzen F *Phys. Rev. D* **90** 043005 (2014)
184. Murase K, Waxman E *Phys. Rev. D* **94** 103006 (2016)
185. Ando S, Feyereisen M R, Fornasa M *Phys. Rev. D* **95** 103003 (2017)
186. Aartsen M G et al. *Eur. Phys. J. C* **79** 234 (2019)
187. Neronov A, Semikoz D *J. Exp. Theor. Phys.* **131** 265 (2020); *Zh. Eksp. Teor. Fiz.* **158** 295 (2020)
188. Yuan C, Murase K, Mészáros P *Astrophys. J.* **890** 25 (2020)
189. Capel F, Mortlock D J, Finley C *Phys. Rev. D* **101** 123017 (2020)
190. Mertsch P, Rameez M, Tamborra I *JCAP* **2017** (03) 011 (2017)
191. Aartsen M G et al. *JCAP* **2020** (07) 042 (2020)
192. Fang K et al. *Astrophys. J.* **894** 112 (2020)
193. Berezinsky V, in *Proc. of the Intern. Conf. on Neutrino Physics and Neutrino Astrophysics, Baksan Valley, 18–24 June, 1977* (Moscow: Nauka, 1978)
194. Eichler D *Astrophys. J.* **232** 106 (1979)
195. Berezinskii V S, Ginzburg V L *Mon. Not. R. Astron. Soc.* **194** 3 (1981)
196. Murase K, in *Neutrino Astronomy Current Status, Future Prospects* (Eds T Gaisser, A Karle) (Singapore: World Sci. Publ., 2017) p. 15
197. Mészáros P *Annu. Rev. Nucl. Part. Sci.* **67** 45 (2017)
198. Böttcher M *Galaxies* **7** 20 (2019)
199. Cerruti M *J. Phys. Conf. Ser.* **1468** 012094 (2020); in *Proc. of the 16th Intern. Conf. on Topics in Astroparticle and Underground Physics, TAUP 2019, Toyama, September 9–13, 2019*; arXiv:1912.03666
200. Begelman M C, Rudak B, Sikora M *Astrophys. J.* **362** 38 (1990)
201. Stecker F W et al. *Phys. Rev. Lett.* **66** 2697 (1991)
202. Stecker F W et al. *Phys. Rev. Lett.* **69** 2738 (1992) Erratum
203. Mannheim K, Stanev T, Biermann P L *Astron. Astrophys.* **260** L1 (1992)
204. Neronov A Yu, Semikoz D V *Phys. Rev. D* **66** 123003 (2002)
205. Stecker F W *Phys. Rev. D* **88** 047301 (2013)
206. Dermer C D, Murase K, Inoue Y *J. High Energy Astrophys.* **3–4** 29 (2014)
207. Kalashev O, Semikoz D, Tkachev I *J. Exp. Theor. Phys.* **120** 541 (2015); *Zh. Eksp. Teor. Fiz.* **147** 614 (2015)
208. Ptitsyna K, Neronov A *Astron. Astrophys.* **593** A8 (2016)
209. Inoue Y et al. *Astrophys. J.* **880** 40 (2019)
210. Murase K, Kimura S S, Mészáros P *Phys. Rev. Lett.* **125** 011101 (2020)
211. Kheirandish A, Murase K, Kimura S S *Astrophys. J.* **922** 45 (2021)
212. Inoue Y, Khangulyan D, Doi A *Galaxies* **9** 36 (2021)
213. Halzen F, Zas E *Astrophys. J.* **488** 669 (1997)
214. Atoyan A, Dermer C D *Phys. Rev. Lett.* **87** 221102 (2001)
215. Bykov A et al. *Space Sci. Rev.* **173** 309 (2012)
216. Sironi L, Spitkovsky A *Astrophys. J.* **698** 1523 (2009)
217. Lemoine M, Waxman E *JCAP* **2009** (11) 009 (2009)
218. Neronov A, Semikoz D *JETP Lett.* **113** 69 (2021); *Pis'ma Zh. Eksp. Teor. Fiz.* **113** 77 (2021)
219. Loeb A, Waxman E *JCAP* **2006** (05) 003 (2006)
220. Bechtol K et al. *Astrophys. J.* **836** 47 (2017)
221. Kistler M D, arXiv:1511.01530
222. Murase K, Inoue S, Nagataki S *Astrophys. J. Lett.* **689** L105 (2008)
223. Kotera K et al. *Astrophys. J.* **707** 370 (2009)
224. Fang K, Murase K *Nat. Phys.* **14** 396 (2018)
225. Murase K *PoS* **ICRC2019** 965 (2020)
226. Ambrosone A et al. *Mon. Not. R. Astron. Soc.* **503** 4032 (2021)
227. Mészáros P, Waxman E *Phys. Rev. Lett.* **87** 171102 (2001)
228. Razzaque S, Mészáros P, Waxman E *Phys. Rev. Lett.* **93** 181101 (2004)
229. Razzaque S, Mészáros P, Waxman E *Phys. Rev. Lett.* **94** 109903 (2005) Erratum
230. Ando S, Beacom J F *Phys. Rev. Lett.* **95** 061103 (2005)
231. Gupta N, Zhang B *Astropart. Phys.* **27** 386 (2007)
232. Murase K, Ioka K *Phys. Rev. Lett.* **111** 121102 (2013)
233. Bhattacharya A et al. *JCAP* **2015** (06) 034 (2015)
234. Tamborra I, Ando S *Phys. Rev. D* **93** 053010 (2016)
235. Senno N, Murase K, Mészáros P *Phys. Rev. D* **93** 083003 (2016)
236. Xiao D et al. *Astrophys. J.* **826** 133 (2016)
237. Denton P B, Tamborra I *JCAP* **2018** (04) 058 (2018)
238. He H N et al. *Astrophys. J.* **856** 119 (2018)
239. Ahlers M, Halser L *Mon. Not. R. Astron. Soc.* **490** 4935 (2019)
240. Wang X-Y et al. *Phys. Rev. D* **84** 081301 (2011)
241. Wang X-Y, Liu R-Y *Phys. Rev. D* **93** 083005 (2016)
242. Dai L, Fang K *Mon. Not. R. Astron. Soc.* **469** 1354 (2017)
243. Senno N, Murase K, Meszaros P *Astrophys. J.* **838** 3 (2017)
244. Lunardini C, Winter W *Phys. Rev. D* **95** 123001 (2017)
245. Guépin C et al. *Astron. Astrophys.* **616** A179 (2018)
246. Guépin C et al. *Astron. Astrophys.* **636** C3 (2020) Erratum
247. Biehl D et al. *Sci. Rep.* **8** 10828 (2018)
248. Murase K et al. *Astrophys. J.* **902** 108 (2020)
249. Gupta A et al. *Astrophys. J. Lett.* **756** L8 (2012)
250. Martynenko N, arXiv:2105.02557
251. Feldmann R, Hooper D, Gnedin N Y *Astrophys. J.* **763** 21 (2013)
252. Taylor A M, Gabici S, Aharonian F *Phys. Rev. D* **89** 103003 (2014)
253. Kalashev O, Troitsky S *Phys. Rev. D* **94** 063013 (2016)
254. Recchia S et al. *Astrophys. J.* **914** 135 (2021)
255. Bertone G, Tait T M P *Nature* **562** 51 (2018)
256. Frampton P H, Glashow S L *Phys. Rev. Lett.* **44** 1481 (1980)
257. Ellis J R, Gaisser T K, Steigman G *Nucl. Phys. B* **177** 427 (1981)
258. Ellis J R et al. *Nucl. Phys. B* **373** 399 (1992)
259. Berezinsky V S *Nucl. Phys. B* **380** 478 (1992)
260. Berezinsky V, Kachelrieß M, Vilenkin A *Phys. Rev. Lett.* **79** 4302 (1997)
261. Kuzmin V A, Rubakov V A *Phys. Atom. Nucl.* **61** 1028 (1998); *Yad. Fiz.* **61** 1122 (1998)
262. Feldstein B et al. *Phys. Rev. D* **88** 015004 (2013)
263. Esmaili A, Serpico P D *JCAP* **2013** (11) 054 (2013)
264. Argüelles C A, Kheirandish A, Vincent A C *Phys. Rev. Lett.* **119** 201801 (2017)
265. Sui Y, Bhupal Dev P S *JCAP* **2018** (07) 020 (2018)
266. Berghaus K V, Diamond M D, Kaplan D E *J. High Energy Phys.* **2019** (05) 145 (2019)
267. Chianese M et al. *JCAP* **2019** (11) 046 (2019)
268. Kuznetsov M Yu *JETP Lett.* **105** 561 (2017); *Pis'ma Zh. Eksp. Teor. Fiz.* **105** 533 (2017)
269. Kachelrieß M, Kalashev O E, Kuznetsov M Yu *Phys. Rev. D* **98** 083016 (2018)
270. Pandey M et al. *Phys. Lett. B* **797** 134910 (2019)
271. Kalashev O, Kuznetsov M, Zhezher Y *JCAP* **2021** (11) 016 (2021)
272. Bykov A M et al. *Mon. Not. R. Astron. Soc.* **453** 113 (2015)
273. Bykov A M *Astron. Astrophys. Rev.* **22** 77 (2014)
274. Bykov A M et al. *Adv. Space Res.* **62** 2764 (2018)
275. Bykov A M et al. *Space Sci. Rev.* **216** 42 (2020)
276. Bouyahiaoui M, Kachelriess M, Semikoz D V *PoS* **ICRC2021** 999 (2021)
277. Bykov A M et al. *Astrophys. J. Lett.* **921** L10 (2021)
278. Gallo Rosso A et al. *Eur. Phys. J. Plus* **133** 267 (2018)